
RESEARCH ARTICLE

GmPIN-dependent polar auxin transport is involved in soybean nodule development

Zhen Gao^{1,2,#}, Zhiwei Chen^{1,2,#}, Yuanyuan Cui^{1,2,#}, Meiyu Ke^{2,3,#}, Huifang Xu^{2,3}, Qinzen Xu^{4,5}, Jiaomei Chen², Yang Li⁶, Laimei Huang², Hong Zhao², Dingquan Huang², Siyuan Mai^{2,3}, Tao Xu^{2,3}, Xiao Liu^{4,5}, Shujia Li⁷, Yuefeng Guan², Wenqiang Yang^{4,5}, Jiří Friml⁸, Jan Petrášek⁹, Jing Zhang⁶ and Xu Chen^{2,*}

¹ College of Resources and Environment, Fujian Agriculture and Forestry University, Fuzhou, Fujian 350002, China.

² Haixia Institute of Science and Technology, Horticultural Plant Biology and Metabolomics Center, Fujian Agriculture and Forestry University, Fuzhou, Fujian 350002, China.

³ College of Life Science, Fujian Agriculture and Forestry University, Fuzhou, Fujian 350002, China.

⁴ Key Laboratory of Photobiology, Institute of Botany, Chinese Academy of Sciences, Beijing 100093, China.

⁵ University of Chinese Academy of Sciences, Beijing 100049, China.

⁶ State Key Laboratory of Plant Physiology and Biochemistry, College of Biological Sciences, China Agricultural University, Beijing 100193, China.

⁷ State Key Laboratory of Plant Genomics and National Center for Plant Gene Research, Institute of Genetics and Developmental Biology, Chinese Academy of Sciences, Beijing 100101, China.

⁸ Institute of Science and Technology Austria (IST Austria), Am Campus 1, 3400 Klosterneuburg, Austria.

⁹ Institute of Experimental Botany of the Czech Academy of Sciences, Prague, Czech Republic.

* Correspondence: Xu Chen (chenxu@fafu.edu.cn)

These authors contributed equally to this work.

Short title: Auxin transport regulates soybean nodule formation

One-sentence summary: In soybean, nodule primordium formation involves GmPIN1-mediated polar auxin transport within primordium cells, and nodule enlargement involves the collaboration of GmPIN9d and GmPIN1-dependent auxin transport within nodule vasculature.

The author responsible for distribution of materials integral to the findings presented in this article in accordance with the policy described in the Instructions for Authors (<https://academic.oup.com/plcell/pages/General-Instructions>) is Xu Chen (chenxu@fafu.edu.cn).

1 ABSTRACT

2 To overcome nitrogen deficiency, legume roots establish symbiotic interactions with nitrogen-
3 fixing rhizobia that is fostered in specialized organs (nodules). Similar to other organs, nodule
4 formation is determined by a local maximum of the phytohormone auxin at the primordium
5 site. However, how auxin regulates nodule development remains poorly understood. Here, we
6 found that in soybean, (*Glycine max*), dynamic auxin transport driven by PIN-FORMED (PIN)
7 transporter GmPIN1 is involved in nodule primordium formation. *GmPIN1* was specifically
8 expressed in nodule primordium cells and GmPIN1 was polarly localized in these cells. Two
9 nodulation regulators, (iso)flavonoids trigger expanded distribution of GmPIN1b to root
10 cortical cells, and cytokinin rearranges GmPIN1b polarity. *Gmpin1abc* triple mutants
11 generated with CRISPR-Cas9 showed impaired establishment of auxin maxima in nodule
12 meristems and aberrant divisions in the nodule primordium cells. Moreover, overexpression of
13 *GmPIN1* suppressed nodule primordium initiation. GmPIN9d, an ortholog of *Arabidopsis*
14 *thaliana* PIN2, acts together with GmPIN1 later in nodule development to acropetally transport
15 auxin in vascular bundles, fine-tuning the auxin supply for nodule enlargement. Our findings
16 reveal how PIN-dependent auxin transport modulates different aspects of soybean nodule
17 development and suggest that establishment of auxin gradient is a prerequisite for the proper
18 interaction between legumes and rhizobia.

19

20 INTRODUCTION

21 The developmental plasticity of plant cells depends largely on de-novo post-embryonic
22 generation of new organs initiated from specialized tissues (Benkova et al., 2003; Yamaguchi
23 et al., 2013; Qi et al., 2014). For example, a lateral root is generated from pericycle cells, via a
24 series of anticlinal divisions, giving rise to lateral root primordia (Benkova and Bielach, 2010).
25 Leaf bulges formed at the flanks of the shoot apical meristem generate leaf primordia (Xiong
26 and Jiao, 2019). Some primordia differentiate into determinate organs with constant cell
27 numbers, whereas others develop into indeterminate organs with a secondary meristem at the
28 tip.

29 Initiation and positioning of an organ primordium is often instructed by local
30 accumulation of the phytohormone auxin (Benkova et al., 2003; Qi et al., 2014; Wu et al.,
31 2015). Local auxin accumulation within founder cells depends mainly on the coordinated
32 activities of AUXIN1/LIKE-AUXIN1 influx carriers and PIN-FORMED (PIN) efflux carriers
33 in conjunction with other auxin transporters (Mravec et al., 2008). The roles of different PINs
34 are well characterized in the context of auxin transport for organ growth and development in

35 *Arabidopsis thaliana*, such as PIN1 in flower development (Okada et al., 1991), PIN2 in root
36 gravitropism (Muller et al., 1998), PIN3 in shoot tropism (Friml et al., 2002), PIN4 and PIN7
37 in embryo development (Benkova et al., 2003; Weijers et al., 2005).

38 The cellular polarity of PIN proteins is tightly related to the direction of auxin flow.
39 For example, primary root growth requires the acropetal/rootward direction of auxin transport
40 by PIN1 which targets the basal side of the plasma membrane (PM) in stele cells, and the
41 basipetal/shootward direction of auxin transport by PIN2 that targets the apical side of PM in
42 epidermal cells, as well as the coordination of PIN3, PIN4 and PIN7 for auxin lateralization
43 within root stem cells (Feraru and Friml, 2008). Current models in diverse organ patterning
44 explicitly show that a PIN-dependent local auxin gradient participates in nearly all types of
45 organ development processes in plants (Benkova et al., 2003; Wisniewska et al., 2006).

46 Many legumes (Fabaceae) are capable of symbiotic interaction with soil bacteria (rhizobia)
47 in specialized organs, called nitrogen-fixing root nodules. The initiation of nodules is triggered
48 by specific signaling molecules, lipochitooligosaccharides (LCOs)/Nod factor released by
49 rhizobia, in response to flavonoids secreted from the root hairs of host plants (Suzaki and
50 Kawaguchi, 2014). Subsequently, the rhizobia penetrate the root via an infection thread,
51 reaching the cortex cells through the curled root hairs. In the cortical cells, the rhizobia
52 stimulate cell proliferation and expansion, resulting in a functional nodule on the host root
53 (Popp and Ott, 2011). Later, the entire nodule is surrounded by a continuum of vascular
54 bundles, providing a robust route to exchange water and organic materials between the root
55 and nodule (Livingston et al., 2019). Within the nodule, rhizobia reside as intracellular
56 symbionts, where they convert atmospheric nitrogen into ammonia to overcome nitrogen
57 shortage in the host plant.

58 Different legume species show substantial variation in nodule organogenesis and nodules
59 are broadly defined as indeterminate versus determinate types. *Medicago truncatula* develops
60 indeterminate nodules, which harbor active apical meristems that continuously produce new
61 meristem tissue. *Lotus japonicus* and *Glycine max* (soybean) generate determinate nodules,
62 whose meristematic activity is lost soon after their initiation (Popp and Ott, 2011). Irrespective
63 of nodule type, these nodules all initiate from a primordium and subsequently develop into
64 diverse organ morphologies. Auxin accumulates at the position of future primordia, to
65 prepare/prime the initiation of nodule primordia (van Noorden et al., 2007; Suzaki et al., 2012;
66 Turner et al., 2013). In soybean, accumulating evidence further illustrates the importance of
67 auxin for nodule development. For example, overexpression of a nodule-expressed auxin
68 biosynthesis enzyme *YUCCA2a* (*GmYUC2a*) delays nodule organogenesis (Wang et al., 2019).

69 Moreover, overexpression of the auxin receptor *TRANSPORT INHIBITOR RESPONSE1*
70 (*GmTIR1*) and suppression of *AUXIN RESPONSE FACTOR8* (*GmARF8*) increases rhizobia
71 infection events and nodule number (Wang et al., 2015b; Cai et al., 2017). Besides many
72 similarities between determinate nodule formation in soybean and *L. japonicus*, species-
73 specific variation exists, such as the pseudoinfections in soybean (Calvert et al., 1984).

74 It has long been proposed that the auxin maximum in the founder cells of a nodule
75 primordium is controlled by polar auxin transport (Hirsch et al., 1989; Mathesius et al., 1998;
76 Kohlen et al., 2018); however, the underlying molecular mechanisms remain elusive. Ng and
77 Mathesius (2018) utilized *L. japonicus* and *M. truncatula* as model legumes to study the
78 differential regulation of auxin transport for initiating determinate and indeterminate nodules.
79 They proposed that acropetal auxin transport is not necessary for determinate nodule formation,
80 based on the observation that acropetal auxin transport in the equivalent root segments below
81 the rhizobia-inoculation spot decreases significantly in *M. truncatula*, while it increases in *L.*
82 *japonicus* (Pacios-Bras et al., 2003; Ng et al., 2015; Ng and Mathesius, 2018). This was further
83 supported the generation of a pseudonodule in *M. truncatula*, but not in *L. japonicus* upon
84 application of auxin transport inhibitors (Ng and Mathesius, 2018). Therefore, the mechanism
85 of determinate nodule formation is somehow different from that of the indeterminate type. So
86 far, much of our knowledge of the regulation of auxin for nodulation derives from the studies
87 of indeterminate nodule development and the knowledge gleaned from lateral root
88 organogenesis. In contrast, the functionality of auxin transport during determinate nodule
89 development remains speculative (Kohlen et al., 2018). Therefore, a better understanding of
90 the PIN-dependent auxin transport module for soybean nodule organogenesis is crucial for
91 discerning the basic nodulation mechanisms and uncovering the different regulatory
92 mechanisms between determinate and indeterminate nodule development.

93 In this study, we demonstrate that soybean nodule primordium formation involves
94 GmPIN1-mediated polar auxin transport. Among all canonical PINs, the GmPIN1 orthologs,
95 *GmPIN1b*, *c*, *d* were specially expressed in nodule primordium cells during nodule primordium
96 initiation, and their dynamic polarity indicate involvement in the directional auxin flux for
97 nodule primordium formation. We found that the upstream nodulation elicitors, flavonoids,
98 trigger the expanding distribution of stele-restricted *GmPIN1b* to cortical cells and cytokinin
99 enable the rapid redirection of the auxin stream by rearranging the cellular GmPIN1b polarity.
100 CRISPR/Cas9-based mutagenesis of *GmPIN1a*, *GmPIN1b* and *GmPIN1c* failed to establish a
101 focused auxin maximum in nodule meristem, resulting in aberrant cortical cell division.
102 Additionally, we found that the soybean-evolved *GmPIN9d* accumulates strongly in the

103 conjunctive vascular bundles between the root and nodule. In these tissues, GmPIN9d acts
104 synergistically with GmPIN1 to coordinate the auxin supply within the vasculature for nodule
105 enlargement. Our findings reveal the fundamental role of GmPIN-dependent polar auxin
106 transport for determinate nodule development.

107

108 **RESULTS**

109 **Auxin accumulates in the nodule primordium and vascular bundles**

110 To visualize the developmental process of soybean nodulation, 7-day-old soybean seedlings
111 were inoculated with the rhizobium strain *Bradyrhizobium* sp. (*BXYD3*). The root segments
112 below shoot-root junction area where large amounts of nodules accumulated (Supp. Fig. S1A)
113 were collected in series for further sectioning, at 4 days post-rhizobia inoculation (dpi) until 14
114 dpi.

115 On the basis of cell morphology, we divided nodule development into four stages. At
116 stage I, rhizobial infection via the curled root hairs determined the position of future nodule
117 primordia and subsequently resulted in cell proliferation in the outer cortex cells,
118 corresponding to nodule primordium initiation. At stage II, cortical cells underwent a series of
119 anticlinal and periclinal divisions to establish a multi-layered meristem. In particular, the
120 soybean nodule primordium started from the outer cortex layer and proceeded both outwards
121 and inwards, suggesting the presence of a dynamic regulator involved in modulating this dual
122 directional cell division. At stage III, the developing nodule continued to produce new cells,
123 and the protruding meristem contained a small amount of bacteroids and visible vascular
124 tissues that connected the host root and nodule. At maturity (stage IV), the oval nodule was
125 rapidly expanding and became filled with large amount of bacteroids, with complex vascular
126 bundles enveloping the entire nodule (Fig. 1A).

127 To track auxin distribution at different growth stages of soybean nodules, we generated
128 a stable transgenic soybean line with the synthetic *DR5-V2-GUS* auxin response reporter (Liao
129 et al., 2015) that shows higher sensitivity to endogenous auxin responses in Arabidopsis than
130 the original *DR5-GUS* reporter (Ulmasov et al., 1997). A robust auxin gradient with a peak
131 concentration at the tip of the nodule primordium, suggesting an early auxin response,
132 coincides with initial cell divisions of the nodule (Fig. 1B, stage I). When the outer cortex cells
133 were rapidly dividing and expanding, we found an accumulation of DR5-V2 activity with its
134 maximum at the apex of the nodule primordium (Fig. 1B, stage II). Afterwards, the tip-focused
135 auxin maximum disappeared and a new auxin maximum gradually appeared within the
136 surrounding cells near the root-nodule vascular connection (Fig. 1B, stage III). Within the

137 rapidly expanding stage IV nodule, auxin was concentrated throughout the nodule vascular
138 bundles (Fig. 1B).

139 The auxin transport inhibitor N-1-naphthylphthalamic acid (NPA) directly elicits the
140 generation of nodule-like structures (pseudonodules) in legume species with indeterminate
141 nodules (Hirsch et al., 1989; Wu et al., 1996; Rightmyer and Long, 2011), but not in those
142 forming determinate nodules (Ng and Mathesius, 2018). We investigated whether NPA
143 influences soybean nodule formation. Therefore, we incubated the rhizobium-colonized *DR5-*
144 *V2-GUS* seedlings with NPA. NPA blocked auxin efflux and disrupted the auxin gradient,
145 resulting in a strong ectopic *DR5-V2* activity around the cortical cells (stage I), pericycle cells
146 (stage II) and vascular bundles (stage III) (Fig. 1B). A reduced auxin response in the central
147 zone of Stage III primordium was observed (Fig. 1B), suggesting a redirection of auxin
148 transport occurs at this stage of nodule development. Interestingly, this was not seen in the
149 NPA-treated plant nodules at the same stage. This ectopic NPA-driven auxin response
150 activation was associated with onset of rapid cell divisions, resulted in a three-fold increase of
151 small nodules compared to the mock treatment (Fig. 1A, Supp. Fig. S1B-D). Additionally,
152 NPA disrupted vascular development, leading to aberrant nodules and two infection zones
153 within bacteroids (Fig. 1A, stage IV). Collectively, these results suggest that nodule
154 primordium formation requires the establishment of an appropriate auxin gradient and the
155 further nodule development of the nodule vascular bundles involves a dynamic redirection of
156 the auxin transport.

157

158 **Identification of nodule-expressed *GmPINs***

159 The best-characterized regulators of auxin transport are PIN efflux transporters (Petrasek et al.,
160 2006). The Arabidopsis PIN family consists of eight members, divided into canonical and non-
161 canonical types based on the length of their hydrophilic loop and subcellular localization
162 (Viaene et al., 2013). The canonical, PM-localized PINs play a predominant role in determining
163 the directionality of intercellular auxin flow (Adamowski and Friml, 2015). To better
164 understand the regulatory mechanism of auxin transport for nodule development, we were
165 motivated to study the functionality of nodule-expressed canonical *GmPIN* ortholog. In
166 soybean, the PIN family has extensively expanded because of the two whole-genome
167 duplication events. A total of 23 *GmPINs* have been identified in the soybean genome, of which
168 seven pairs of the duplicated genes, namely the *GmPIN1*, *GmPIN2*, *GmPIN3*, *GmPIN5*,
169 *GmPIN6*, *GmPIN8* and *GmPIN9* subfamilies (Wang et al., 2015a). According to the
170 constructed phylogenetic tree, the canonical *GmPIN* members comprise *GmPIN1* (*GmPIN1a*,

171 *b, c, d, e*), *GmPIN2* (*GmPIN2a, b*), and *GmPIN3* (*GmPIN3a, b, c, d*), which showed the highest
 172 sequence similarity with Arabidopsis *AtPIN1*, *AtPIN2*, and *AtPIN3*, 4, 7, respectively (Fig. 2A,
 173 Supplemental File 1). Additionally, the soybean genome contains a specific *GmPIN9* group
 174 that has apparently co-evolved with *GmPIN2* (Fig. 2A, Supplemental File 1&2).

175 To search for nodule-expressed *GmPINs*, we extracted RNA from nodules at 14 dpi to
 176 perform reverse transcription quantitative PCR (RT-qPCR). Among the 23 *GmPINs*, the
 177 canonical PIN orthologs, *GmPIN1*, *GmPIN2*, *GmPIN3* genes were detectable in the mature
 178 nodule. Additionally, *GmPIN5a* and *GmPIN9d* transcripts were strikingly abundant in the
 179 mature nodule, suggesting their possible involvement as well (Fig. 2B). The hydrophilic loop
 180 of *GmPIN9* is shorter than the canonical PINs but longer than that of the non-canonical type
 181 (Supp. Fig. S2A); hence, the functionality of *GmPIN9* during nodule development deserved
 182 our further investigation.

183

184 **GmPIN1, orthologs of auxin efflux carrier AtPIN1, control directional auxin flow for** 185 **nodule primordium formation**

186 We first examined the expression profiles of canonical *GmPINs* during nodule development,
 187 including *GmPIN1*, *GmPIN2* and *GmPIN3*. We established *pGmPIN1a-e:GUS*, *pGmPIN2a-*
 188 *b:GUS* and *pGmPIN3a-d:GUS* constructs, using a reporter gene encoding β -glucuronidase
 189 (GUS) individually driven by an approximately 2-kb region upstream of the *GmPIN* coding
 190 sequence. We then introduced them into soybean seedlings via hairy root transformation.
 191 Histochemical staining of the root tip revealed that every *GmPIN1* was expressed in the root
 192 stele, consistent with the expression pattern of *AtPIN1* in Arabidopsis root (Supp. Fig. S3A).

193 Upon rhizobial infection, expression of the *GmPIN1b, c, d* reporters was detected in the
 194 nascent nodule primordia that formed in outer cortical cells (Fig. 2C). After a series of cortical
 195 cell divisions, the primordium tip-distributed *GmPIN1b, c, d* gradually accumulated in the
 196 surrounding vascular bundles (Fig. 2C). In stage IV, the expression of *GmPIN1b, c, d* were
 197 confined to vascular bundles (Fig. 2C). By contrast, *GmPIN1a* appeared after primordium
 198 emergence and its expression was exclusively associated with vascular bundle development,
 199 whereas *GmPIN1e* had an extremely weak signal in nodule primordia (Fig. 2C). *GmPIN1*
 200 expression was associated with the nodule primordium and the nodule vascular bundle (Fig.
 201 2D), consistent with the spatial pattern of auxin activity during nodule development. This
 202 suggested the possible involvement of *GmPIN1* in nodulation.

203 Other *GmPIN* members, *GmPIN2a* and *2b* were mainly expressed in root epidermis
 204 and outer cortex cells, and *GmPIN3a-d* genes were expressed in root vascular cells (Supp. Fig.

205 S3B). By contrast, both *GmPIN2* and *GmPIN3* mainly accumulated in nodule vascular bundles
206 after establishment of the nodule primordium; only *GmPIN2a* and *GmPIN3a* were detectable
207 in the nodule primordium tip, albeit at extremely low levels (Supp. Fig. S3B). Our analysis of
208 the spatio-temporal expression pattern of canonical *GmPINs* lent further support for a
209 predominant role of GmPIN1 in nodule development.

210 The variation in the expression of multiple *GmPIN1* orthologs allowed us to evaluate
211 the functional conservation between GmPIN1 and AtPIN1. We established a GmPIN1-GFP
212 fusion protein under the control of the *AtPIN1* promoter. We cloned GFP in-frame in the
213 hydrophilic loop of GmPIN1 (Fig. 3A) at the comparable position, as in AtPIN1-GFP
214 (Benkova et al., 2003; Wisniewska et al., 2006) and introduced them into the Arabidopsis *pin1-
215 En* mutant. All the transgenic Arabidopsis *pAtPIN1:GmPIN1a-e-GFP* plants showed partial
216 rescue of the pin-shaped inflorescence meristem phenotype of the homozygous *pin1*
217 (Galweiler et al., 1998), in that they had a high percentage of normal growing stems with intact
218 flowers and siliques (Fig. 3C). In the root stele, protein localization of GmPIN1a-e was
219 confined to the basal side of PM (Fig. 3B), consistent with the subcellular polarity of AtPIN1.
220 To further confirm the cellular polarity of GmPIN1a-e, we also generated transgenic
221 Arabidopsis plants having *GmPIN1a-e-GFP* driven by their native *GmPIN1a-e* promoters.
222 Similar to *pAtPIN1:GmPIN1-GFP* or in *pGmPIN1:GmPIN1-GFP* transgenic seedlings,
223 GmPIN1a-e were exclusively confined to the basal PM in root stele cells (Supp. Fig. S3C),
224 thus indicating the conservation of localization between GmPIN1 and AtPIN1 proteins.

225 On the basis of this functional conservation and consistent polarization of the five
226 GmPIN1 proteins, we next focused on GmPIN1b because it was detectable throughout all
227 stages of nodule development, using it as a representative to study the dynamics of GmPIN1
228 polarity during nodule development. For this, we generated a stable transgenic soybean line
229 transformed with *pGmPIN1b:GmPIN1b-GFP*. By comparison with wild-type (WT) plants, we
230 were able to distinguish the GFP signal from the strong auto-fluorescence of soybean tissues
231 under the same fluorescence microscopy settings (Supp. Fig. S4). We determined the degree
232 of polar localization of GmPIN1b as the signal ratio of apical relative to lateral side of
233 individual cells (called the polarity index, p.i.) (Fig. 3G). In the soybean root stele, GmPIN1b
234 displayed basal polarity (p.i.=2.6), consistent with its distribution in Arabidopsis (Fig. 3D, G).
235 During the nodule primordium initiation (stage I) with visible anticlinal cell divisions,
236 GmPIN1b showed predominant polarization towards the future nodule meristem (p.i.=3.2);
237 while some of the cells exhibited dual polarization of GmPIN1b, with PM accumulation
238 towards the imminently initiated nodule vascular bundle and towards the primary root tip (Fig.

239 3D, G). The predominant apical polarity of GmPIN1b towards the primordium apex suggests
240 that auxin is being transported to nodule primordia, while the bi-polar localization of GmPIN1b
241 implies that auxin is partly being directed away from the outer cortical cells.

242 In stage II, GmPIN1b polarity was mainly directed to the protruding nodule primordium
243 (p.i.=2.2); while a proportion of primordia cells displayed the lateral polarity of GmPIN1b,
244 which might result in reduced auxin response at the nodule primordium tip (Fig. 3D, 3G, Supp.
245 Fig. S5A). When the nodule primordium was fully established (stage III), GmPIN1b polarized
246 towards the primordium tip as well as in the lateral direction (p.i.=1.7) (Fig. 3D, 3G, Supp. Fig.
247 S5A), suggesting that GmPIN1 established a re-allocation route for draining auxin away from
248 the tip region. In the mature nodule (stage IV), the GmPIN1b-GFP signal was restricted within
249 vascular bundles (Fig. 3D, G), corresponding to the depletion of auxin at the primordium tip
250 and its reallocation to the vascular bundles (Fig. 1B).

251 We further examined whether GmPIN1b directs auxin flow toward the central cells of
252 the nodule primordium or away to the peripheral cells by evaluation of apical or lateral
253 GmPIN1b signal at stages I, II and III. Compared to the GmPIN1b signal in stage I, the apical
254 direction of the GmPIN1b signal was significantly reduced to 53% and 62% in stage II and
255 stage III+IV, while the lateral GmPIN1b signal was not promoted in the later stages (Fig. 3F).
256 The comparison of GmPIN1b polarization at different stages of nodule development further
257 indicated that the re-allocation of auxin away from nodule primordium tip is caused by the
258 reduction of apical polarization of GmPIN1.

259 In vascular bundles of mature nodules, GmPIN1b was highly polarized within the
260 differentiated vasculature (p.i.=21.0) but was non-polar within the undifferentiated vasculature
261 (p.i.=1.0, Fig. 3D, G). The polarization of GmPIN1b within the mature vasculature of root-
262 nodule junction suggested that auxin might be directionally transported via the nodule
263 vasculature. Interestingly, GmPIN1b polarity was disrupted by NPA. NPA relocated the
264 GmPIN1b polarity to the lateral side that was perpendicular to nodule primordium cells
265 (p.i.=1.4 in NPA-treated nodule primordia, compared to p.i.=2.3 in the untreated ones) (Fig.
266 3E-G, Supp. Fig. S5B). Consequently, NPA-rearranged GmPIN1 polarity resulted in ectopic
267 formation of nodule primordia (Fig. 1A, 3E). Taken together, the dynamic polarization of
268 GmPIN1 in the nodule primordium is consistent with the presence of multiple cell proliferation
269 sites during soybean determinate nodule development, which begins in the outer cortex and
270 proceeds outwards as well as inwards.

271

272 **GmPIN1s regulate nodule primordium formation**

273 Soybean has evolved five *PINI* orthologues compared with the sole *PINI* identified in
274 Arabidopsis, suggesting a functional redundancy of *GmPIN1* genes. Among them, *GmPIN1a*,
275 *b* and *c* showed the closest sequence similarity to *AtPIN1* (Fig. 2A), while *GmPIN1d* and *e*
276 might be an ancestral PIN1 form (Kohlen et al., 2018). Using the CRISPR/Cas9 approach, we
277 designed a sgRNA that simultaneously edits the first exon of *GmPIN1a*, *b* and *c*, from which,
278 we subsequently obtained two independent, triple mutants of *Gmpin1abc* (named *Gmpin1abc*-
279 L1 and -L2) via *Agrobacterium*-mediated stable transformation in soybean (Fig. 4A). These
280 *Gmpin1abc* mutants displayed slightly shorter primary roots, fewer lateral roots, and had less
281 biomass in their shoot tissues, compared to WT (Supp. Fig. S6A-D).

282 To understand the contribution of GmPIN1 to auxin transport, we examined the auxin
283 transport capacity in *Gmpin1abc* mutants. Without rhizobium inoculation, *Gmpin1abc* mutants'
284 acropetal auxin transport was reduced by 89%, compared to WT (Fig. 5H). The decreased
285 acropetal auxin transport in *Gmpin1abc* mutants resulted in strongly reduced auxin content
286 (46%-53%) compared to WT, and a reduced *DR5-V2-GUS* activity (Supp. Fig. S6E, F).
287 Quantification of the total nodule number (per plant) and nodule density (nodule number per
288 cm² of root area) both demonstrated that *Gmpin1abc* had fewer nodules than the WT (Fig. 4B,
289 C, E). Despite the reduction in nodulation events in *Gmpin1abc* mutants, their average nodule
290 size was not significantly changed, as indicated by diameter distribution profile of more than
291 1000 nodules (Fig. 4D, F). The nodulation phenotype of the *Gmpin1abc* mutant indicates that
292 GmPIN1 is involved in regulation of nodule formation.

293 We then generated stable transgenic plants that constitutively overexpressed *GmPIN1a*-
294 *c* (*35s:GmPIN1a-c*). The *35s:GmPIN1a-c* lines all exhibited curling roots and an unusual
295 thickening of hypocotyls (Supp. Fig. S7A, B), features similar but not entirely identical to
296 agravitropic root growth seen in Arabidopsis *35s:AtPIN1* plants (Zhang et al., 2010). Further
297 analysis of nodulation phenotypes showed that the induction of *GmPIN1a*, *b* and *c* all
298 significantly reduced nodule size (Fig. 4G-J). The retarded growth of *35s:GmPIN1* nodules
299 could be due to the disrupted auxin maximum at nodule primordia, leading to delayed
300 organogenesis, or due to an impaired auxin concentration within the enlarged nodule that
301 impeded nodule expansion.

302 To understand the causal relationship of the defective nodulation phenotype in
303 *Gmpin1abc* mutants and gain-of-function *GmPIN1* lines, we examined the density of nodule
304 primordia at 5 dpi, when most of the nodules had just emerged as primordia. We divided the
305 nodules into two categories: primordia (without the resident bacteroids) and developing
306 nodules (with bacteroids). Compared with WT, *Gmpin1abc* mutants had a significantly

307 decreased density of nodule primordia but this did not influence their developing nodules (Fig.
308 5A-C), further supporting the involvement of GmPIN1 in nodule primordium formation.
309 Strikingly, *35s:GmPIN1a* has almost no detectable nodule primordia at 5 dpi (Fig. 5A-C, I).

310 To further understand the functionality of GmPIN1-mediated auxin transport during
311 nodule primordium formation, we established a spot inoculation system in soybean (Fig. 5D)
312 to closely examine auxin transport efficiency and nodule primordium morphology within the
313 spot inoculation area. To this end, 0.5-cm root segments of WT and *Gmpin1abc* mutants below
314 the root-shoot junction were subjected to a continuous *BXYD3* spot inoculation for 48h (Fig.
315 5D, Supp. Fig. S7C). Auxin concentration was individually measured in the above (upper, U)
316 and below (lower, L) root segments close to the inoculated site. In WT, rhizobial infection did
317 not influence auxin levels in upper root segments, but decreased the auxin content to 72% in
318 the lower segments, compared to the uninfected roots (Fig. 5G). Auxin concentration was
319 generally decreased in *Gmpin1abc* roots, compared to WT. In *Gmpin1abc* mutants, rhizobial
320 inoculation did not change auxin level in the upper root segments but caused auxin elevation
321 in the lower segments (247% and 196%) (Fig. 5G).

322 The opposite responsiveness of WT and *Gmpin1abc* intrigued us to further examine
323 auxin transport rates of inoculated root segments. Radiolabeled [³H]-IAA was applied to the
324 upper segments and the transported [³H]-IAA was measured in the lower segments at 48 hours
325 post inoculation (hpi). In WT or *Gmpin1abc-L2* mutants, rhizobial inoculation did not
326 significantly change the efficiency of acropetal auxin transport across the inoculated roots (Fig.
327 5H). It is worth noting that rhizobial inoculation tended to decrease auxin transport in WT
328 (92%), while it tended to increase auxin transport in *Gmpin1abc-L1* and *L2* mutants (121% and
329 111%), compared to the uninfected samples (Fig. 5H). Reduction of auxin levels below the
330 inoculation site supported the notion that auxin transport regulation happens prior to the
331 formation of visible nodule primordia. Whereas, the minor change of acropetal auxin transport
332 upon rhizobium infection suggested that nodule primordium initiation in the outer cortex is not
333 sufficient to influence acropetal auxin transport within the primary root vasculature. The
334 unexpected elevation of auxin level in lower segments of *Gmpin1abc* suggests that a possible
335 upregulation of auxin biosynthesis occurs within inoculated-*Gmpin1abc* roots.

336 We further examined nodule primordium morphology at 5 days after rhizobia spot-
337 inoculation. The visible nodule primordium with a series of anticlinal and periclinal divisions
338 were homogenously distributed in inoculated WT root segments, while clusters of aberrantly
339 dividing cortical cells and nodule primordia were discretely distributed in *Gmpin1abc* mutants
340 (Fig. 5E), compared to the normal cortical cells in the uninfected roots (Supp. Fig. S7D). We

341 then introduced *DR5-V2-GUS* in WT, *Gmpin1abc* mutants and *35s:GmPIN1a* to visualize the
342 auxin distribution. A robust auxin gradient with a peak concentration was present at the tip of
343 WT nodule primordium (stage I) (Fig. 5F). Despite the *DR5-V2* signal remaining clear in
344 nodule primordium of *Gmpin1abc* mutant, the mutant failed to establish a focused auxin
345 gradient in the primordium apex (stage I) (Fig. 5F). The defective auxin maximum in
346 *Gmpin1abc* resulted in the ectopic formation of nodule primordia, leading to the clustered
347 spacing of nodule primordia. By contrast, overexpression of *GmPIN1a* in *35s:GmPIN1a* roots
348 resulted in ectopic auxin deposition in the cells beneath the primordium tip, which interfered
349 with the directional auxin transport that would guide nodule primordia to grow outwards.
350 Consequently, *35s:GmPIN1a* exhibited a delay in nodule organogenesis (Fig. 5A, F). These
351 results collectively demonstrate that a GmPIN1-mediated auxin gradient regulates nodule
352 primordium formation.

353

354 **Flavonoids and cytokinin influence PIN1 distribution and polar localization during** 355 **nodulation**

356 An auxin maximum and *GmPIN1b, c, d* expression emerged in nodule primordium founder
357 cells, suggesting the involvement of auxin transport in the initial step of nodule formation.
358 However, *GmPIN1a, b, c* expression was exclusively restricted within the root vasculature
359 (Supp. Fig. S3A), which pointed to an unknown nodulation signal eliciting the lateralization of
360 GmPIN1 to prime the auxin signal at these founder cells.

361 Flavonoids are crucial signaling molecules that can trigger the synthesis of Nod factors
362 from rhizobia, ensuring successful symbiotic infection of host plant tissues (Liu and Murray,
363 2016). A variety of flavonoid compounds have been characterized, and most of them act as
364 inhibitors of auxin transport (Brown et al., 2001; Santelia et al., 2008; Ng et al., 2015) by
365 interfering with PIN expression and its polar localization (Peer et al., 2004; Santelia et al., 2008;
366 Kuhn et al., 2017). According to the multiple steps of signal exchange during nodule formation,
367 different flavonoids may play distinct roles across individual steps of nodulation (Zhang et al.,
368 2009). The isoflavone compound genistein is a well-characterized Nod-factor inducer in
369 soybean (Ip et al., 2001; Subramanian et al., 2006; Lang et al., 2008). We thus checked the
370 effect of genistein on the expression pattern of *GmPIN1b*, serving as a representative *GmPIN1*.
371 Soybean plants with *pGmPIN1b:GUS* showed an expanded distribution of *GmPIN1b* into their
372 cortical cells by genistein treatment (Supp. Fig. S8A, C). The flavonoid 7,4'-dihydroxyflavone
373 (DHF) is a Nod gene-inducing flavone compound in *M. truncatula*, known to function very
374 early during nodulation (Zhang et al., 2009). Application of exogenous DHF to soybean

375 *pGmPIN1b:GUS* trans-genetic plants also showed an expanded distribution of *GmPIN1b* into
376 the cortical cells (Supp. Fig. S8A, C), consistent with the genistein treatment. These results
377 indicated that the isoflavone genistein and flavonoid DHF affect GmPIN1 distribution.
378 Corresponding to the expanded distribution of GmPIN1b, genistein and DHF treatment
379 resulted in a significantly increased *DR5-V2-GUS* signal along the outer cortex and epidermal
380 cells, but a decrease in quiescent center of root tip (Supp. Fig. S8B, D). These data collectively
381 demonstrate that the isoflavone/flavonoid influences GmPIN1 distribution and auxin
382 accumulation, and probably leading to the alteration of auxin transport during nodulation.

383 Appropriate integration of various phytohormones is essential for determining when
384 and where organogenesis occurs, such as the coordination between auxin and cytokinin
385 (Schaller et al., 2015; Pierre-Jerome et al., 2018; Kurepa et al., 2019). Cytokinin plays a major
386 role in the control of cortical cell divisions during nodule primordium formation (Murray et al.,
387 2007; Reid et al., 2017), which consequently promotes nodule numbers (Supp. Fig. S9A, B).
388 To understand whether cytokinin functions upstream of auxin, we applied a synthetic cytokinin,
389 6-benzylaminopurine (6-BA), onto *pGmPIN1b:GmPIN1b-GFP*. Visualization of GmPIN1b
390 localization revealed that 6-BA rearranged the cellular GmPIN1b polarity that predominantly
391 targeted to primordium tip, resulting in a switch of GmPIN1b polarity to the lateral side that
392 was perpendicular to the primordium cells (Fig. 6A, B). Cytokinin-mediated directional
393 alteration of PIN polarity during nodule meristem formation was consistent with its effect on
394 lateral root initiation (Marhavy et al., 2014). Interestingly, a directional alteration of GmPIN1
395 polarity by 6-BA treatment resulted in a series proliferation in the outer cortical cells of WT
396 plants, comparable with the cell morphology in spot inoculated-*Gmpin1abc* mutants (Fig. 6C,
397 5G). Hence, these findings suggested that cytokinin-regulated re-polarization action of
398 GmPIN1 might facilitate a rapid auxin stream redirection, which provides an efficient approach
399 to initiate nodule primordium. Taken together, the influence of flavonoid and cytokinin on
400 GmPIN1 cellular localization might coordinate an appropriate auxin gradient for nodule
401 organogenesis.

402

403 **GmPIN9d is a nodule vascular bundle-abundant auxin transporter**

404 The above results confirmed the important role of GmPIN1 during nodule primordium
405 formation. Apart from the typical canonical and non-canonical GmPINs, there was an
406 additional GmPIN9 subfamily conspicuously present in soybean that showed a very close
407 evolutionary relationship with the PIN2 clade (Fig. 2A). Our RT-qPCR analysis of *GmPIN9a-*
408 *d* expression levels showed that *GmPIN9d* was extremely enriched in the mature nodule (Fig.

409 7C). In contrast, the transcripts of *GmPIN9a*, *GmPIN9b*, *GmPIN9c* were rather low or not
410 detectable (Fig. 7C), making GmPIN9d the most likely candidate involved in nodulation.

411 We next generated a stable transgenic soybean plant with a GUS reporter gene driven
412 by the 2-kb promoter region of *GmPIN9d*. A series of cross-sections spanning leaf to root
413 tissues, integrated with histochemical staining, from 10-day-old *pGmPIN9d:GUS* seedlings
414 demonstrated that *GmPIN9d* was weakly expressed in aerial tissues but enriched in both root
415 and nodule. Either in the hypocotyl or root organs, *GmPIN9d* was confined within the vascular
416 bundles (Fig. 7A, B). Histochemical co-staining of xylem cells using phloroglucinol confirmed
417 that *GmPIN9d* was located in protoxylem cells (Fig. 7A). Intriguingly, *GmPIN9d* was
418 particularly abundant in the conjunctive vascular bundles lying between the root and nodule
419 (Fig. 7B), which suggested a potential role of GmPIN9d in the later stage of nodule growth
420 when primordia were already established.

421 Because GmPIN9d is a soybean-evolved PIN, we tested if GmPIN9d is indeed a
422 functional auxin transporter. To do this, we cloned GmPIN9d-GFP under control of the
423 Arabidopsis PIN2 promoter (*pAtPIN2:GmPIN9d-GFP*) and introduced it in the Arabidopsis
424 PIN2 knockout mutant, *eir1-4* that showed agravitropic roots (Muller et al., 1998). Compared
425 to *pAtPIN2:GmPIN2b-GFP* which entirely rescued the agravitropic root phenotype of *eir1-4*
426 mutant, *pAtPIN2:GmPIN9d-GFP* displayed a partial restoration (Supp. Fig. S11A-C),
427 suggesting that GmPIN9d might carry out a comparable function as PIN2 protein for polar
428 auxin transport. Importantly, much of the GmPIN9d-GFP localized to the internal structures
429 reminiscent of the endoplasmic reticulum (ER) (Supp. Fig. S11B), suggesting that it either acts
430 at the ER, or that its trafficking to the membrane is impaired in Arabidopsis.

431 We further generated *Gmpin9d* mutants using CRISPR/Cas9. Two homozygote mutant
432 alleles were identified, designated *Gmpin9d-#1* and *9d-#2*, with an early stop codon that arose
433 from a 2-bp and 40-bp deletion, respectively (Fig. 8A). The 7-day-old *Gmpin9d* mutants had
434 slightly decreased length and density of lateral roots, but did not display other obvious
435 developmental defects in adult plants (Fig. 8B, Supp. Fig. S10A-C). Next, the auxin response
436 reporter *DR5-V2-GUS* was introduced to hairy roots of the WT and the *Gmpin9d* mutant. The
437 *DR5-V2-GUS* activity was much reduced in both the roots and nodules of *Gmpin9d* mutant
438 (Fig. 8C), supporting the involvement of GmPIN9d in auxin homeostasis.

439 The GmPIN9 clade is located between canonical and non-canonical PIN types,
440 according to our phylogenetic analysis (Fig. 2A). This raised a problem: might GmPIN9d
441 polarly transport auxin as a canonical PIN, or does it regulate auxin homeostasis as a non-
442 canonical PIN? To address these questions, we measured free and conjugated auxin levels in

443 both the WT and *Gmpin9d* mutants, using High-Performance Liquid Chromatography (HPLC).
444 In comparison to WT, the free auxin level decreased by approximately 50% in roots and 20%
445 in nodules of *Gmpin9d* mutants (Fig. 8G-H), results consistent with the previous observation
446 of *DR5-V2* activity (Fig. 8C). However, the conjugated form of auxin, indole-3-acetyl-aspartate
447 (IAA-asp), in *Gmpin9d* mutants occurred at a level comparable to WT (Supp. Fig. S10D-E),
448 supporting a transporter function of GmPIN9d. Finally, using radiolabeled [³H]-IAA, we
449 measured the auxin transport capacity of GmPIN9d in 2-cm equivalent root segments of the
450 WT and *Gmpin9d* mutants. Both *Gmpin9d-#1* and *#2* mutants underwent a significant decrease
451 in auxin transport in the rootward (acropetal) but not shootward (basipetal) direction, in
452 comparison with WT (Fig. 8D-F). Altogether, these results show that GmPIN9d can transport
453 auxin to the root tip.

454

455 **GmPIN9d-dependent auxin transport is required for nodule enlargement**

456 Although the free auxin level was diminished by approximately 50% in roots of *Gmpin9d*
457 compared to WT, the density of nodules and nodule primordia were not significantly changed
458 (Fig. 8I-J). However, the profile of nodule size in *Gmpin9d* was slightly shifted compared to
459 WT (Fig. 8K), suggesting the involvement of GmPIN9d for nodule expansion. Still, the
460 phenotypic defects of *Gmpin9d* single mutants were mild might be caused by complicated gene
461 redundancy of PIN family. The acropetal auxin transport capacity of GmPIN9d was
462 reminiscent of GmPIN1, prompting us to speculate that GmPIN9d might work synergistically
463 with GmPIN1 to achieve polar auxin transport within nodule vascular bundles.

464 We then examined the subcellular localization of GmPIN9d, via visualization of the
465 Arabidopsis transgenic *pAtPIN2:GmPIN9d-GFP* seedlings. GmPIN9d showed dual
466 localization in both ER and PM by colocalization of GmPIN9d-GFP with FM4-64-stained PM
467 and HDEL-labelled ER (Supp. Fig. S11D-E). PM-associated PIN proteins are located on the
468 PM, meanwhile be trafficking among endomembrane system via endocytosis and exocytosis
469 pathways (Chen et al., 2011; Adamowski and Friml, 2015).

470 To further investigate whether GmPIN9d is associated with the PM, we applied
471 Brefeldin A (BFA), which is widely used as a vesicle trafficking inhibitor (Geldner et al., 2003).
472 BFA specifically blocks exocytosis but allows endocytosis, aggregating both secretory and
473 endocytic endomembrane cargoes in BFA bodies. BFA treatment specifically aggregated the
474 PM-localized GmPIN2b, but not the ER-resident AtPIN8 in BFA bodies (Supp. Fig. S11F).
475 We found that BFA also resulted in the aggregation of GmPIN9d proteins within BFA

476 compartments (Supp. Fig. S11F). These data in Arabidopsis clearly evinced a dual localization
477 of GmPIN9d in both PM and ER, similar to AtPIN6.

478 We further detected the *in vivo* distribution of GmPIN9d in soybean roots and nodules,
479 by placing the GmPIN9d-GFP fusion protein under the control of the native GmPIN9d
480 promoter (Fig. 9A). The transformed positive hairy roots were selected based on a dTomato
481 fluorescence-based screening system (Supp. Fig. S12A). In *pGmPIN9d:GmPIN9d-GFP*
482 positive hairy roots, a strong GFP signal was present in the root protoxylem, with rootward PM
483 localization (Fig. 9B). In particular, this GmPIN9d-GFP signal was associated with vascular
484 bundles within the nodule and root-nodule conjunction. The strong polarization of GmPIN9d
485 within root-nodule conjunctive vasculature suggested its possible involvement in directing
486 auxin stream towards nodule (Fig. 9B, Supp. Fig. S11G). Such a GmPIN9d polarized pattern
487 resembles GmPIN1 at a later stage of nodule development, pointing to their synergistic activity.
488 Hence, we introduced the *Gmpin9d-RNAi* construct in *Gmpin1abc* triple mutants via the
489 dTomato-based hairy root screening system. The resulting *Gmpin1abc Gmpin9d-RNAi* showed
490 a comparable nodule density but much smaller nodule size than *Gmpin1abc* (Fig. 9C-E, Supp.
491 Fig. S12B-D). Taken together, the above results demonstrated that GmPIN9d-dependent polar
492 auxin transport functions at the later stage of nodule development, collaborating with GmPIN1
493 to fine-tune nodule enlargement.

494 **DISCUSSION**

495 Legume plants interact with rhizobia to generate nodule organs, representing a way by which
496 legume species coordinate the mutually beneficial exchange of signals and nutrients with their
497 symbiotic partners. Previous studies have characterized well the crucial roles of Nod factor
498 recognition, nodule inception (NIN) transcription factor, and phytohormone cytokinin in
499 nodule formation (Ng et al., 2015; Schiessl et al., 2019; Bozsoki et al., 2020; Laffont et al.,
500 2020). Here, we showed that dynamic GmPIN1 polarization establishes auxin canalization
501 during nodule primordium development; flavonoids influence GmPIN1 distribution and
502 cytokinin rearranges the cellular GmPIN1 polarity, participating in auxin gradient formation.
503 The later stage of nodule enlargement involves the collaboration of GmPIN9d and GmPIN1-
504 dependent auxin transport within nodule vasculature (Fig. 9F). Our data thus provide insights
505 into auxin-regulated nodule development in legume plants.

506

507 **Establishment of an auxin maximum is required for determinate nodule primordium**
508 **formation**

509 Auxin accumulation appears in the early stage during nodule primordium formation, when the
510 rhizobia-elicited infection threads start to grow in the proliferating cortical cells of *L. japonicus*
511 (Suzaki et al., 2012), suggesting that nodule primordium formation is tightly accompanied by
512 an auxin response. In soybean, overexpression of a nodule-expressed auxin biosynthesis
513 enzyme *GmYUC2a* increases auxin content by approximately two fold, but severely delays
514 nodule formation (Wang et al., 2019). These data suggests that maintenance of appropriate
515 auxin concentration and distribution is a prerequisite for determinate nodule primordium
516 formation. If auxin transport is not required for determinate nodule primordium formation,
517 there should be a burst of local auxin biosynthesis at the nodule primordium site. YUCCA
518 flavin monooxygenases are the major enzymes catalyzing IAA synthesis (Mashiguchi et al.,
519 2011; Stepanova et al., 2011; Zhao, 2018). In soybean, *GmYUC2a* is the most abundant nodule-
520 expressed YUC among all GmYUCs (Wang et al., 2019); however, *GmYUC2a* displays
521 uniformly high activity in all participating cell layers during nodulation, including the root
522 hairs, proliferating cortex cells, and nitrogen fixation zone (Wang et al., 2019). It is unlikely
523 that a localized auxin maximum, restricted to nodule primordium founder cells, can be
524 established solely relying on GmYUC2a. PIN-mediated polar auxin transport has been well
525 characterized and deemed necessary for almost all organogenesis processes in plants. This
526 raises the hypothesis that PIN-mediated auxin transport could also contribute to formation of
527 determinate nodules.

528 Subramanian and colleagues mentioned that no measurable inhibition of auxin
529 transport occurred at the site of rhizobial inoculation where flavonoids/isoflavonoids
530 accumulate in soybean root, and they concluded that the effects of flavonoids on auxin
531 redistribution is not required for soybean nodulation (Subramanian et al., 2007). Our study
532 confirmed that acropetal auxin transport is not significantly affected in the rhizobia-inoculated
533 root segments (Fig. 5H). Different kinds of flavonoids are synthesized at distinct stages of
534 nodule formation (Mathesius et al., 1998), and the fluorescent flavonoids were visualized in
535 different cell layers of distinct legumes. For instance, flavonoids were found in the inner
536 cortical cells of pea (*Pisum sativum*) and alfalfa (*Medicago sativa*), but they were found in the
537 outer cortical cells of siratro (*Macroptilium atropurpureum*) (Mathesius et al., 1998). These
538 data suggest that different flavonoids play diverse roles during different stages of nodule
539 formation and in different species of legume plants.

540 Flavonoids have a general inhibitory effect on auxin transport (Buer et al., 2013; Ng et
541 al., 2015; Zhang et al., 2021), and acropetal auxin transport was disrupted during indeterminate
542 nodule formation where high amounts of flavonoids were synthesized. However, soybean
543 nodules initiate in the cells of outer cortex, and flavonoid compounds are probably also
544 synthesized at the outer cortex of soybean roots, lying far from the phloem. This could explain
545 why acropetal auxin transport is not affected during nodule primordium formation in soybean.
546 To understand whether flavonoid-mediated auxin inhibition is a necessary step for nodule
547 primordium initiation in soybean, it is necessary to closely examine GmPIN1 distribution and
548 auxin gradient in weak alleles of isoflavone synthase (IFS) or chalcone synthase (CHS)
549 mutagenized soybean plants within nodule primordium cells. Despite flavonoids being the best
550 candidates to prime the auxin signal, an obvious question remains unresolved. Soybean nodule
551 are initiated at the outer cortex cells, while *L. japonicus* nodule are initiated at the inner cortex
552 cells and the *M. truncatula* nodule begins from the pericycle, endodermis and cortex cells
553 (Gauthier-Coles et al., 2018). So, how does the deposition of flavonoids in different cell layers
554 in different kinds of legume plants modulate PINs and auxin transport?

555 In the present study, we demonstrate that a PIN-dependent auxin transport module
556 participates in soybean nodule primordium formation. *GmPIN1b, c, d* target to the founder
557 cells of nodule primordia, reallocating the auxin stream towards the nodule primordium and
558 flows away from the primordium. A proposed mathematic model postulates that nodule
559 formation is associated with the reduction of PIN function and an increase of auxin
560 concentration in all root cell layers (Xiao et al., 2014). Nevertheless, this auxin-involved
561 nodulation module is based on specific auxin accumulation from the inner to outer cell layers;

562 hence, the proliferation of cortex cells should start from the interior layers and proceed
563 outwards (Xiao et al., 2014). Yet, the determinate nodule exhibits dual directions of cell
564 proliferation, in that it begins from cortex cells and proceeds outwards as well as inwards.
565 Therefore, only the initial steps of nodule primordium development (proceed outwards) fit with
566 the proposed model (Xiao et al., 2014).

567 NPA disrupts auxin gradient formation during nodule primordium formation. In stage
568 I, auxin accumulates with its maximum at the nodule primordium apex, compared with a bulk
569 deposition of auxin along the dividing cortical cells in NPA-treated group; in stage II and III,
570 auxin response gradually reduces from the nodule primordium apex, compared with an ectopic
571 auxin accumulation in and around the dividing cortical cells (Fig. 1B). Together, the three-fold
572 increase of small nodules in NPA-treated roots indicates that disruption of auxin efflux by NPA
573 causes ectopic nodule primordium formation. Similar to the NPA treatment, loss of
574 *GmPIN1ABC* impairs polar auxin transport, generating clusters of abnormal dividing cells and
575 defective nodule primordia after continuous rhizobial inoculation (Fig. 5E). Hence,
576 establishment of an appropriate auxin gradient is a prerequisite to control nodule primordia
577 positioning. Whereas, nodule number was promoted in NPA-treated roots, which was opposite
578 with the consequence of decreased nodules in *Gmpin1abc* mutants. NPA directly associates
579 with PINs, and it inhibits PINs activity by stabilizing PIN1, PIN2, PIN3, PIN4 and PIN7
580 homo- and heteromers in Arabidopsis (Abas et al., 2021; Teale et al., 2021). Apparently, NPA
581 not only inhibits GmPIN1 activity, but also functions on other GmPINs. Hence, NPA-induced
582 nodules might be caused by the additive effects of NPA on all GmPIN proteins.

583

584 **Auxin supply is involved in nodule enlargement**

585 Despite acropetal auxin transport capacity and auxin concentration being severely decreased
586 in the root and nodule of the *Gmpin9d* single mutant, it did not display significant defects in
587 nodulation. A plausible explanation for this is that GmPIN9d functions at later stages of
588 nodulation where it is highly redundant with other PINs, including GmPIN1, GmPIN2 and
589 GmPIN3. Mutagenesis of multiple *GmPINs* recently became possible via CRISPR/Cas9. After
590 nodule primordia are formed, auxin maxima are rapidly concentrated within nodule vascular
591 bundles, suggesting an additive effect of other auxin transporters for auxin canalization
592 between the primordium and vascular bundles. Therefore, the nodule-expressed *GmPIN2* and
593 *GmPIN3* might also participate in later stages of nodule development. The fundamental effect
594 of auxin has been well known to stimulate cell expansion (Du et al., 2020). Hence, auxin stream

595 in vascular bundles could be a source of auxin to maintain auxin supply within the developing
596 nodule, modulating nodule enlargement.

597

598 MATERIALS AND METHODS

599

600

601 Plant growth and phenotype analysis

602 Soybean (*Glycine max*) cultivar Williams 82 and Huachun6, and *Arabidopsis thaliana*

603 *Columbia-0* were used as wild type (WT). Seeds of *Arabidopsis thaliana* were sown on 0.8%

604 agar containing 1/2 Murashige and Skoog media at 22°C under 16h light/ 8h dark photoperiod.

605 Soybean seeds were germinated in vermiculite. To analyze nodulation phenotype, 7-day-old

606 plants were inoculated with *Bradyrhizobium sp. (BXYD3)* which was re-suspended in low-

607 nitrogen buffer (530 µM N, including KNO₃, NH₄NO₃, Ca(NO₃)₂•4H₂O, and

608 (NH₄)₂SO₄(15:4:12:3), and 1.2 mM CaCl₂, 1.05 mM K₂SO₄, 0.5 mM MgSO₄•7H₂O, 25 µM

609 MgCl₂, 2.5 µM NaB₄O₇•10H₂O, 0.5 µM MnSO₄•H₂O, 1.5 µM ZnSO₄•7H₂O, 0.5 µM

610 CuSO₄•5H₂O, 0.15 µM (NH₄)₆Mo₇O₂₄•4H₂O, 40 µM Fe-Na-EDTA, 250 µM KH₂PO₄) to

611 OD₆₀₀=0.15 for 2 h, then these inoculated plants were transferred to soil (vermiculite, and

612 irrigated with low-nitrogen buffer) for an additional 14 days (25°C, 14h light/ 10h dark

613 photoperiod). Light growth condition for soybean plants is white light added with blue and red

614 LEDs, the light intensity is 13000 LUX (measured by an HR-350 Light Meter; Hipoint). The

615 resultant plants were collected for nodule number and density quantification by ImageJ.

616 For NPA treatment, soybean seeds were germinated in vermiculite. 7-day-old plants

617 were inoculated with *BXYD3* (OD₆₀₀≅1.0) which was re-suspended in low-nitrogen buffer

618 for 2 h, then the inoculated plants were transferred to low-nitrogen hydroponic solution with

619 or without 1-N-naphthylphthalamic acid (NPA) (10⁻⁷ M) for additional 21 days. Nodules were

620 harvested and analyzed.

621 For DHF, genistein or 6-BA chemical treatments, DHF and genistein were dissolved in

622 DMSO, and 6-BA was dissolved in NaOH as stock solutions. 7-day-old seedlings were

623 irrigated by chemical-containing low-nitrogen solution.

624

625 RNA extraction and RT-qPCR analysis

626 RNA was extracted using the TransZol Up Plus RNA kit (TransGen Biotech), and the first-

627 strand cDNA was synthesized using TransScript All-in-One SuperMix (TransGen Biotech).

628 qRT-PCR was performed using a Bio-Rad CFX96 real-time system (Bio-Rad) with 20 µL

629 volumes containing 2 μ L of 1:5 diluted reverse transcription product, 0.8 μ L of specific primers,
630 7.2 μ L of ddH₂O, and 10 μ L of 2 \times TransStart Green qPCR SuperMix (TransGen Biotech). The
631 housekeeping gene *GmActin-11* was used as a reference and relative expression levels of each
632 gene were calculated using the $2^{-\Delta\Delta CT}$ method. All primers used in this study are listed in
633 Supplemental Table S1.

634

635 **Phylogenetics and motif analysis**

636 *Arabidopsis thaliana* *PIN* genes were obtained from TAIR (<http://www.arabidopsis.org>).
637 Soybean *PIN* genes were obtained from Phytozome (<https://phytozome.jgi.doe.gov>).
638 *Klebsormidium flaccidum* *PIN* (*KfPIN*) was obtained from Genbank
639 (<https://www.ncbi.nlm.nih.gov>). *PIN* genes were translated into protein sequences and aligned
640 with Clustal X (Larkin et al., 2007). Phylogenetic analysis was constructed using MEGA X
641 with neighbor-joining (NJ) criteria and verified using the maximum likelihood (ML) method
642 (Kumar et al., 2018), and 1000 bootstrap replicates were performed based on the multiple
643 alignments of the protein sequences encoded by *PIN* genes. NJ analysis was performed using
644 the protein Poisson distances and the pairwise deletion of gap sites. The default parameters
645 were used for ML analysis. Moreover, Phylogenetics conserved motifs were detected in *PIN*
646 members using the motif analysis tool MEME (<http://meme-suite.org/tools/meme>) (Bailey et
647 al., 2009) with the default parameters except for maximum number of motifs, 25. The *PIN*
648 sequence alignment is provided as Supplemental File S1 and a machine-readable alignment is
649 provided as Supplemental File S2.

650

651 **Used primers, vectors and cloning strategy**

652 Promoter fragments of *GmPIN9d* (2003bp), *GmPIN1a* (2132bp), *GmPIN1b* (2043bp)
653 *GmPIN1c* (1917bp) *GmPIN1d* (1809bp) and *GmPIN1e* (1476bp) were amplified from
654 Williams 82 genomic DNA. The fragments were cloned into pDONR221 using Gateway BP
655 Clonase II enzyme mix and recombined into the pGWB633 Gateway destination vector by LR
656 reaction to create *pGmPIN:GUS* (primers are provided in Supplemental Table S1). To create
657 *pAtPIN1:GmPIN1a-e-GFP*, *pGmPIN1a-e:GmPIN1a-e-GFP*, *pGmPIN9d:GmPIN9d-GFP*,
658 *pAtPIN2:GmPIN2b-GFP* and *pAtPIN2:GmPIN9d-GFP*, the insertion site of GFP was
659 described in previous studies (Benkova et al., 2003; Xu and Scheres, 2005; Wisniewska et al.,
660 2006). GFP was inserted into the genomic fragments at position 1646 (after ATG) in *GmPIN9d*,
661 at position 1680 in *GmPIN2b*, at position 1396 in *GmPIN1a*, at position 1547 in *GmPIN1b*, at

662 position 1407 in *GmPIN1c*, at position 1914 in *GmPIN1d* and at position 1904 in *GmPIN1e*.
663 Genomic DNA of *GmPINs* and *GFP* were cloned into pBGWK by infusion clone technology.

664 To generate *Gmpin1abc* triple mutant and *GmPIN9d* single mutant, sgRNA was
665 designed according to the prediction from CRISPR-GE (<http://skl.scau.edu.cn/home/>). sgRNA
666 cloning approach was performed as described previously (Bai et al., 2020). To generate the
667 constructs with modified dTomato-tag, dTomato fragment was amplified using the primers of
668 pGmEF1A-dTomato F2 and R2, which was driven by the promoter of pGmEF1a; Tnos
669 fragment was amplified using the primers of pGmEF1A-dTomato F3 and R3. Then, pGmEF1a,
670 dTomato and Tnos were assembled by Goldengate assembly kit using BsaI and T4 ligase.
671 Finally, pGmEF1a-dTomato fragments were assembled with other fragments to create
672 destination vectors via Goldengate cloning methods. All strategies of vectors and cloning used
673 in this study are listed in Supplemental Table S2. Locus numbers of *GmPIN* genes are listed in
674 Supplemental Table S3. Amino acid information of GmPIN proteins are listed in Supplemental
675 Table S4.

676

677 **Rhizogenes-mediated hairy root transformation**

678 Rhizogenes-mediated hairy root transformation was carried out as described before (Kereszt et
679 al., 2007). *Agrobacterium* strain K599 carrying the constructs was directly injected into the
680 hypocotyl proximal to the cotyledon of the 5-day-old healthy soybean seedlings. The infected
681 plants were grown under high humidity condition until hairy roots emerged in high-nitrogen
682 hydroponic solution (contains 5.3 mM nitrogen including KNO₃, NH₄NO₃, Ca(NO₃)₂•4H₂O,
683 (15:4:12), and 0.3 mM K₂SO₄, 0.5 mM MgSO₄•7H₂O, 25 μM MgCl₂, 2.5 μM NaB₄O₇•10H₂O,
684 0.5 μM MnSO₄•H₂O, 1.5 μM ZnSO₄•7H₂O, 0.5 μM CuSO₄•5H₂O, 0.15 μM
685 (NH₄)₆Mo₇O₂₄•4H₂O, 40 μM Fe-Na-EDTA, 250 μM KH₂PO₄). After the primary roots were
686 removed, the plants with the hairy roots were transferred into fresh wet vermiculite with
687 irrigation of low-nitrogen buffer, and further inoculated with rhizobium strain *BXYD3* for
688 additional 14 days growth. The positive hairy roots with dTomato fluorescence were selected
689 by hand-held lamp with 555nm excitation laser.

690

691 **Rhizobial spot inoculation**

692 5-day-old soybean seedlings were used for spot inoculation in low-nitrogen hydroponic system.
693 0.5cm root segments below the root-shoot junction were covered by humid foam with *BXYD3*
694 (OD₆₀₀ ≥ 1.0) by continuous spot inoculation for 48h (equipped as shown in Fig. 5D). 3cm

695 foam (keep humid with low-nitrogen buffer) was wrapped above the inoculation site to keep
696 roots humid. Auxin concentration was measured in the above (upper, U) and below (lower, L)
697 root segments close to the inoculated site, and auxin transport was measured across the spot
698 inoculation site at 48 hpi.

699

700 **Generation of stable transgenic soybean plants**

701 For soybean stable plant transformation, the established constructs were transformed into the
702 *Agrobacterium tumefaciens* strain *EHA101* or *GV3101*. *Gmpin9d* mutant was generated in
703 Williams 82 ecotype, *Gmpin1abc* mutant and *35s:GmPIN1* lines were generated in *Huachun6*
704 ecotype. Transformants were established and screened by PCR amplification using primers for
705 basta and the corresponding genes (Supplemental Table S1).

706

707 **Histochemical GUS staining**

708 GUS staining solution contains 50 mM sodium phosphate buffer (pH 7.0), 0.1% (v/v) Triton
709 X-100, 0.1 mM $K_3Fe(CN)_6$, 0.1 mM $K_4[Fe(CN)_6] \cdot 3H_2O$, 1 mg/mL X-Gluc and 1% (v/v)
710 dimethylformamide. Samples were stained for 1-4 h at 37°C. Chlorophyll was removed by
711 sequential incubations in 50% ethanol, 100% ethanol, and 50% ethanol for several hours at
712 each step. After rehydration, samples were transferred to glass slides with 50% glycerol
713 mounted.

714

715 **Endogenous hormone measurement**

716 Phytohormone extraction and measurement were performed using HPLC as described
717 previously (Yang et al., 2019) with modifications. Briefly, root or nodules were ground to
718 powder in liquid nitrogen. Approximately 100 mg powder with the addition of a mixture of
719 internal standards were extracted with 1 mL of ethyl acetate by vortexed for 10 min and
720 sonicated for 20 min at 4 °C, respectively. After centrifugation at 12000 rpm for 3 min at 4 °C,
721 the supernatant was obtained and then evaporated until dry using a vacuum concentrator
722 (Eppendorf, Germany) at 30 °C. The dried residues were diluted in 500 μ L of 70% methanol
723 and then filtered through a 0.22 mm cellulose acetate filter.

724

725 **Auxin transport measurements**

726 5-day-old seedlings were used to measure the capacity of auxin transport as described
727 previously (Lewis and Muday, 2009) with modifications. The 2cm root segments above the
728 root tip were collected (Fig. 8D). For the measurement of acropetal or basipetal auxin transport,

729 the bottom or top of segmented roots were inserted into the tube that contains a consistent
730 volume of small [³H]-IAA agar block, for 3 h incubation in the dark. 0.5cm root segments just
731 above the inoculation site were excised and washed by 1/2 MS liquid for 15 min. Then, these
732 segments were placed into scintillation vials containing 2 mL of scintillation fluid for 16-24 h.
733 Radioactivity was measured as described previously (Lewis and Muday, 2009), and auxin
734 transport efficiency was calculated according to the method described previously (Lewis and
735 Muday, 2009).

736 For auxin transport measurement in spot inoculation system, 2.5cm root segments
737 below root-shoot junction area were collected (Fig. 5D), the top of segmented roots (U) were
738 inserted into the tube that contains a consistent amount of [³H]-IAA solution, for 3 h incubation
739 in the dark. 0.5cm root segments in L position were collected for radioactivity in scintillation
740 vials containing 1 mL of scintillation fluid for 16-24 h.

741

742 **Tissue slicing and microscopy observation**

743 For resin embedding and sectioning, the different stages of nodules were collected and fixed
744 in Formalin solution, and then dehydrated in a graded alcohol series. The fixed materials were
745 subsequently embedded in Technovit 7100 (Kulzer GmbH) according to the manufacturer's
746 protocol.

747 For pPIN:GUS and PIN-GFP analysis in soybean plants, root segments were collected
748 and embedded within 7-8% agarose. After solidification, the samples were sliced using a Leica
749 RM2255 microtome in transversal or longitudinal directions of 80 µm thickness. For GFP
750 samples, the root/nodule median sections were selected under dissecting microscope with
751 obvious vasculature, and the fluorescence were further observed by confocal microscopy under
752 the same setting. For GUS samples, the slices were further stained by GUS staining solution
753 for 4-8 h, or stained with 0.001% Toluidine Blue O staining for 10-20 seconds. All samples in
754 a single experiment were stained with consistent time.

755 For fluorescence observation, images were taken by either Zeiss LSM 880 (with
756 Airyscan) or Leica SP8 confocal microscopes. The settings of excitation and detection were:
757 GFP: 488 nm, 505-550 nm; FM4-64: 535 nm, 610 nm. All images in a single experiment were
758 captured with the same setting.

759 For nodule primordium assay, 5dpi seedlings were used to quantify the density of
760 nodule primordium. The 1cm root segments were consistently collected from lateral roots in
761 root-shoot junction areas. 5 to 10 individual root segments were collected from each plant, and
762 at least 8 plants were analyzed. For nodule primordium assay in spot inoculation system, root

763 segments were collected from the foam-covered inoculated site. Root sections with 80 μ m
 764 thickness were produced using a vibratome (Leica). The root sections were then stained by
 765 0.25% potassium permanganate for 10-30 seconds and soaked into Schiff's fuchsin-sulfite
 766 solution. Nodule primordium was observed by Nikon Ti-E light microscope and the density
 767 was quantified by ImageJ.

768

769 **Statistical analysis, image analysis and figure preparation**

770 Statistical data were analyzed in Graphpad Prism 7 (GraphPad Software, La Jolla California
 771 USA, www.graphpad.com). Statistical images were generated by Graphpad Prism 7. Camera
 772 and confocal images were prepared with ImageJ (<http://imagej.nih.gov/ij/>). All the experiments
 773 were carried out at least in triplicate.

774

775 **Accession numbers**

776 Soybean gene accession numbers: GmPIN1a (Glyma.08G054700), GmPIN1b
 777 (Glyma.07G102500), GmPIN1c (Glyma.09G176300), GmPIN1d (Glyma.03G126000),
 778 GmPIN1e (Glyma.19G128800), GmPIN2a (Glyma.13G101900), GmPIN2b
 779 (Glyma.17G057300), GmPIN3a (Glyma.07G217900), GmPIN3b (Glyma.20G014300),
 780 GmPIN3c (Glyma.07G164600), GmPIN3d (Glyma.09G117900), GmPIN5a
 781 (Glyma.09G251600), GmPIN5b (Glyma.18G241000), GmPIN6a (Glyma.13G038300),
 782 GmPIN6b (Glyma.14G120900), GmPIN8a (Glyma.05G109800), GmPIN8b
 783 (Glyma.17G157300), GmPIN8c (Glyma.09G240500), GmPIN8d (Glyma.18G255800),
 784 GmPIN9a (Glyma.09G061800), GmPIN9b (Glyma.15G168100), GmPIN9c
 785 (Glyma.09G097300), GmPIN9d (Glyma.15G208600). Arabidopsis PIN accession
 786 numbers: AtPIN1(AT1G73590), AtPIN2(AT5G57090), AtPIN3(AT1G70940),
 787 AtPIN4(AT2G01420), AtPIN5(AT5G16530), AtPIN6(AT1G77110), AtPIN7(AT1G23080),
 788 AtPIN8(AT5G15100). KfPIN:(KJ466099).

789

790 **SUPPLEMENTAL DATA**

791 Supplemental Figure S1. NPA promotes small nodule formation.

792 Supplemental Figure S2. Structure of GmPINs.

793 Supplemental Figure S3. Expression pattern of *GmPINs*.

794 Supplemental Figure S4. Auto-fluorescence in GFP channel in WT roots and nodules.

795 Supplemental Figure S5. GmPIN1b is polarly localized toward nodule primordium apex.

796 Supplemental Figure S6. Phenotype analysis of *Gmpin1abc* triple mutant.

797 Supplemental Figure S7. Phenotype analysis of *GmPIN1* overexpression lines.
798 Supplemental Figure S8. Flavonoids influence GmPIN1b and auxin distribution.
799 Supplemental Figure S9. Cytokinin treatment increases nodule density.
800 Supplemental Figure S10. Conjugated IAA is not influenced in *Gmpin9d* mutants.
801 Supplemental Figure S11. GmPIN9d has a dual cellular localization in both ER and PM.
802 Supplemental Figure S12. dTomato-based hairy root selection system.
803 Supplemental Table S1. Primers used for genotyping and RT-qPCR analysis.
804 Supplemental Table S2. Cloning Strategy.
805 Supplemental Table S3. *GmPIN* gene locus number.
806 Supplemental Table S4 Amino acid information.
807 Supplemental File S1 PIN sequence alignments.
808 Supplemental File S2 Readable tree file.
809

810 **ACKNOWLEDGEMENTS**

811 This work was supported by the National Key Research and Development Program of China
812 (2016YFD0100705 and 2017YFA0506100), the Fok Ying Tung Education Foundation
813 (161027) and Training Program for Excellent Young Scholars of Fujian Agriculture and
814 Forestry University (KSYLX011) to Xu Chen; National Natural Science Foundation of China
815 (31900213), Natural Science Foundation of Fujian (2019J01420) and Distinguished Young
816 Scholar Program of Fujian Agriculture and Forestry University (xjq201921) to Zhen Gao;
817 National Natural Science Foundation of China (32000190) to Dingquan Huang; MEYS project
818 (CZ.02.1.01/0.0/0.0/16_019/0000738) to Jan Petrášek. We thank Hong Liao for the donation
819 of soybean seeds of *Williams 82*, *Huachun6* and rhizobia *Bradyrhizobium sp.*, Le Gao for
820 technical help of soybean transformation, Yonghong Wang for the help of auxin transport
821 measurement, Xiaomin Yu for the technical help of auxin content measurement, Steffen
822 Vanneste for critical reading and language modification, and Zhongquan Lin for microscopy
823 assistance.
824

825 **AUTHOR CONTRIBUTIONS**

826 ZG and XC designed research; ZG, ZC, YC, MK, HX, QX, SM performed the research; ZG
827 contributed new analytic tools; YL, HZ, DH, TX and XL helped the manuscript interpretation
828 and analysed data; LH and JC generated the transgenic soybean plants; YG contributed
829 soybean CRISPR/Cas9 vector; SL, WY, JF, JP and JZ contributed the technical help and

830 helpful discussion; ZG and XC wrote the paper. ZG, ZC, YC and MK contributed equally as
831 co-first authors, and XC contributed as corresponding author.

832

833 **FIGURE LEGENDS**

834 **Figure 1. NPA disrupts auxin distribution and nodule formation.**

835 (A-B) 7-day-old WT (A) or *DR5-V2-GUS* transgenic soybean plants (B) were infected by
836 *BXYD3*, and then incubated in low-nitrogen hydroponic solution containing 10^{-7} M NPA or
837 DMSO (as mock control). Root-shoot junctions were collected in series at 4-14 dpi for resin
838 embedding and sectioning. The morphology of stage I to IV soybean nodules was examined
839 by sectioning in the longitudinal direction (A). Red boxes label the primordium area, dotted
840 lines label the vascular bundles, and black arrows highlight the nodule or nodule primordium
841 (A). *DR5-V2* activity in different nodule stages was stained and captured by sectioning in
842 longitudinal (L) or transverse (T) directions (B). St: root stele. Red dot lines label the sectioning
843 areas in transverse direction. Red arrows highlight the dividing cortical cells. Scale bars, 100
844 μm (A, B).

845 **Figure 2. Expression pattern of *GmPINs* during nodule development.**

846 (A) The phylogenetic tree of PIN proteins from Arabidopsis (At), *Glycine max* (Gm) and
847 *Klebsormidium flaccidum* (Kf) was constructed using MEGA X. These *PIN* genes were
848 grouped as canonical, non-canonical and soybean-specific PIN types.

849 (B) Transcript level of 23 *GmPIN* genes was detected by RT-qPCR in nodules at 14dpi ($n \geq 3$),
850 *Gmactin11* was the normalization gene.

851 (C) *pGmPIN1a, b, c, d, e:GUS* constructs were introduced in WT soybean plants by hairy root
852 transformation, the positive roots were infected by *BXYD3*. Root segments were collected at 4
853 to 14 dpi. Root sectioning was performed for the further histochemical staining.

854 (D) Cartoon model represents the spatial and temporal expression pattern (different colors) of
855 *GmPIN1s* during nodule development.

856 Scale bars, 100 μm (C). Error bar=S.D.

857 **Figure 3. *GmPIN1* localization is conserved with *AtPIN1* and direct auxin flow during 858 nodule primordium formation.**

859 (A) Predicted topology of *GmPIN1* proteins. The following *GmPIN1-GFP* constructs were
860 established based on the insertion position of GFP in the hydrophilic loop.

861 (B-C) *GmPIN1a-e* distribution and polarity were visualized in roots of the transgenic
862 Arabidopsis plants (*pAtPIN1: GmPIN1-GFP* in *pin1-En* Arabidopsis (At.) mutant background
863 (B, C). The phenotypes of inflorescence and silique (inset boxes) were shown in C. Polar

864 localization of GmPIN1 in the basal side of PM in root stele (inset boxes) is highlighted by
865 white arrows (B).

866 (D) GmPIN1b localization was visualized in roots and different stages of nodules in the
867 transgenic soybean plant *pGmPIN1b:GmPIN1b-GFP*. The polarity of GmPIN1b (with
868 predominant polarity toward nodule apex) was highlighted by white arrows. Dot lines label the
869 area of C1-derived cell layers or vascular bundle. Pictures with bright field view were shown
870 in the inset boxes of upper panels. The images in lower panels showed the enlarged views of
871 boxed areas in the representative cartoon (1: undifferentiated vascular bundles; 2 and 3:
872 differentiated vascular bundles). Yellow and blue dotted lines represent GmPIN1b signal on
873 periclinal and anticlinal directions at stage I.

874 (E) GmPIN1b localization was visualized in nodule primordium (stage II) of NPA (10^{-7} M,
875 4days)-treated *pGmPIN1b:GmPIN1b-GFP* seedlings White arrows label GmPIN1b polarity
876 toward nodule apex.

877 (F-G) GmPIN1b signal toward the nodule apex (apical) or perpendicular to the nodule apex
878 (lateral) was individually measured in F (n=136, 189, 89, 129, 136, 189, 89, 129). The
879 comparison ratio of GmPIN1b signal in different nodule primordium stage relative to those in
880 stage I was shown as percentage in F. Polar index of GmPIN1b was quantified by calculation
881 of GmPIN1b signal ratio of apical-targeted GmPIN1b signals relative to them in the lateral
882 sides (G: n=90, 136, 189, 89, 129, 40, 102).

883 Scale bars, 5 μ m (B), 50 μ m (B, inset box), 5mm (C), 100 μ m (D upper panel, E), 20 μ m (D lower
884 panel). Error bar=S.D. In D-E: Ep, epidermis; C1, 1st cortical cell layer; C2, 2nd cortical cell
885 layer; Ed, endodermis; Pc, pericycle; St, stele; VB, vascular bundle. Root tip growth directions
886 (g) were labelled by red arrows (D, E). Nodule primordium apex (apical-targeted GmPIN1b)
887 was labelled by yellow arrows, and the lateral localization (perpendicular to the apical direction)
888 of GmPIN1b was labelled by blue arrows (D, E). P-values were determined by two-tailed
889 Student's t-test assuming equal variances (**p< 0.001; ****p<0.0001; ns, not significant).

890 **Figure 4. Nodulation phenotypes of *Gmpin1abc* triple mutant and *GmPIN1***
891 **overexpression lines.**

892 (A) *Gmpin1abc* triple mutants were generated via CRISPR-Cas9 gene editing approach. The
893 sequence of *GmPIN1a*, *b*, *c* with the gRNA targeted sites was designed in the first exon of
894 *GmPIN1* genes. gRNA targeted sequences were framed by green, and the mutation or deletion
895 sequences were labelled by red. Two independent triple mutant lines with edited genes are
896 shown.

897 (B-J) 7-day-old WT, *Gmpin1abc* mutants and *35s:GmPIN1a, b and c* lines were infected by
 898 *BXYD3*, and the nodulation phenotypes were analyzed at 14 dpi. Nodule number (per plant)
 899 and density (number per cm²) were quantified in C (n=15, 9, 20, 17) and E (n=15, 9, 20, 17).
 900 Profile of nodule diameter was tracked in D (n=2138, 945), F (n=2236, 1404), H (n=848, 930,
 901 480), I (n=1111, 471), J (n=1318, 961, 1096) (all from upper to lower groups).
 902 Scale bars, 1cm (B, G). Error bar=S.D. P-values were determined by two-tailed Student's t-
 903 test assuming equal variances (**p< 0.01; ***p< 0.001).

904 **Figure 5. Loss-of-function and gain-of-function of *GmPIN1* disrupted auxin distribution**
 905 **and nodule primordium initiation.**

906 (A-C, I) 7-day-old WT, *Gmpin1abc-L1* and *35s:GmPIN1a-L11* plants were infected by *BXYD3*
 907 for additional 5 days growth. Consistent 1cm root segments were collected from lateral roots
 908 at the root-shoot junction area. Root segments were sectioned in longitudinal direction and co-
 909 stained by Chameleon and Schiff's fuchsin-sulfite reagents (A). Nodule primordium density
 910 and developing nodule density were individually quantified as profiles in B (n=106) and C
 911 (n=106). The overall nodule primordium density was analyzed in I (n=106). The middle panels
 912 of WT in A show 3× enlarged views of boxed areas in the images of left panels.

913 (D,E-G,H) 0.5cm root segments below root-shoot junction of 5-day-old WT, *Gmpin1abc-L1*
 914 and *Gmpin1abc-L2* were performed by 48h continuous *BXYD3* spot inoculation (equipped as
 915 the cartoon in D). Auxin content in the upper (U) and lower (L) root segments close to the
 916 inoculated position was measured in G (uninfected roots were used as controls) (n=5, 3, 3, 4,
 917 4, 3, 5, 5, 4, 4, 4, 4). Polar auxin transport (PAT) efficiency was measured in the acropetal
 918 direction in H (n=12, 14, 10, 13, 12, 11; red arrow in D labelled PAT direction). The
 919 comparison ratio of auxin content in L relative to those in U is shown as a percentage in G, and
 920 the comparison ratio of auxin transport capacity in infected groups to uninfected groups was
 921 shown as percentage in H. Nodule primordium morphology in WT and *Gmpin1abc* mutants
 922 was observed at 5dpi after spot inoculation (E). Cartoons simulate cell morphology of each
 923 genotype, and green color indicates the dividing cortical cells (E). The percentage in E indicates
 924 the proportion of roots with aberrant dividing cortical cells in the total counting roots.

925 (F) *DR5-V2-GUS* construct was introduced in WT, *Gmpin1abc-L1* and *35s:GmPIN1a-L11*
 926 plants by hairy root transformation, and different stages of nodule were collected at 8dpi for
 927 sectioning. Auxin distribution was visualized by histochemical GUS staining.

928 Scale bars, 200µm (A), 100µm (E, F). Error bar=S.D. P-values were determined by two-tailed
 929 Student's t-test assuming equal variances (*p<0.05; **p< 0.01; ****p< 0.0001; ns, not
 930 significant).

931 **Figure 6. Cytokinin rearranges GmPIN1b polarity.**

932 (A-B) Nodule primordium of *BXYD3*-infected *pGmPIN1b:GmPIN1b-GFP* soybean plants
 933 were analyzed at 8dpi (with or without 1 μ M 6-BA treatment for 16h). GmPIN1b-GFP signal
 934 in the apical (yellow arrows) and lateral (blue arrows) directions of nodule primordium was
 935 calculated and shown as lateral/apical ratio in (B) (n=126 from 22 sections, 152 from 36
 936 sections), and the distribution frequency of GmPIN1b signal ratio was shown in the right chart
 937 (B, grey dot line marked the cutoff value). The cells with GmPIN1b signal ratio above the
 938 cutoff value was highlighted by yellow stars (A). Root tip growth directions (g) were labelled
 939 by red arrows (A).

940 (C) 7-day-old WT plants were infected by *BXYD3*, and then they were irrigated with low-
 941 nitrogen hydroponic solution containing 0.1 μ M 6-BA or DMSO (as mock control) for
 942 additional 7 days. Cortical root cell morphology was observed by root sectioning. Numbers in
 943 the right panels showed 4 \times enlarged views framed in the left image. The percentage indicates
 944 the proportion of roots with a cluster of dividing cortical cells in the total counting roots.
 945 Scale bars, 100 μ m (A), 500 μ m (C). Error bar=S.D. P-values were determined by two-tailed
 946 Student's t-test assuming equal variances (****p<0.0001).

947 **Figure 7. *GmPIN9d* is specifically expressed in the protoxylem cells of vascular bundles
 948 and root-nodule junctions.**

949 (A) Different tissues of 10-day-old *pGmPIN9d:GUS* transgenic soybean plants were in series
 950 collected for sectioning and histochemical staining. Xylem cells were indicated by
 951 phloroglucin co-staining. Numbers in the right and lower panels indicate the areas labelled in
 952 the left image. Pictures in the lower panels showed 3 \times enlarged views of the images in the
 953 upper panels.

954 (B) *pGmPIN9d:GUS* transgenic soybean plants were infected by *BXYD3*, roots and different
 955 stages of nodules were collected for sectioning and histochemical staining.

956 (C) Transcript levels of *GmPIN9a, b, c, d* genes were detected in different soybean tissues by
 957 RT-qPCR, and *Gmactin11* was used as the normalization gene. The relative transcript levels
 958 are shown by heatmap.

959 Scale bars, 100 μ m (A) and 200 μ m (B).

960 **Figure 8. *GmPIN9d* transports auxin in an acropetal direction.**

961 (A) *Gmpin9d* mutants were generated via CRISPR-Cas9 gene editing. gRNA targeted sites of
 962 *GmPIN9d* are framed in green, and the mutation or deletion sequences are labeled in red. Two
 963 independent mutant lines with editing manner were shown.

964 (B) Global morphology of 21-day-old *Gmpin9d* mutants.

965 (C) *DR5-V2-GUS* construct was introduced in WT, *Gmpin9d#2* mutant background by hairy
966 root transformation, and the positive hairy roots were infected by *BXYD3*. Roots and nodules
967 were collected at 14dpi for sectioning and histochemical staining.

968 (D-F) Auxin transport capacity of WT and *Gmpin9d* mutants was assayed in 2cm root segments
969 as described in D, and acropetal and basipetal auxin transportation were tracked by [³H]-IAA
970 (n=9, 12, 6 in E; n=11, 10, 13 in F).

971 (G-H) Free IAA level was individually measured in the roots and nodules of WT and *Gmpin9d*
972 mutants (G: n=12, 15, 11; H: n=15, 15, 15).

973 (I-K) 7-day-old WT and *Gmpin9d* mutants were infected by *BXYD3*. The nodule primordium
974 density was analyzed at 6dpi (I: n=121, 137, 129), the nodule density was measured at 14dpi
975 (J: n=8, 8, 7), and the profile of nodule diameter was tracked (K: n=560, 536, 473).

976 Scale bars, 10cm (B), 100μm (C). Error bar=S.E.M in E-H, S.D. in I, J. P-values were
977 determined by two-tailed Student's t-test assuming equal variances (*p< 0.05; **p< 0.01; ns,
978 not significant).

979 **Figure 9. GmPIN9d works synergistically with GmPIN1 to coordinate nodule**
980 **enlargement.**

981 (A) GmPIN9d-GFP construct was established based on the insertion position of GFP in the
982 hydrophilic loop.

983 (B) *pGmPIN9d:GmPIN9d-GFP* construct was introduced in WT soybean plant by hairy root
984 transformation, and the positive roots were infected by *BXYD3*. Roots and nodules were
985 collected at 14dpi for sectioning, and GmPIN9d-GFP signal was visualized. Cells with polar
986 GmPIN9d are highlighted by white arrows. The numbered images show 5×enlarged views (red
987 boxes) in Supp. Fig. S11G images. Root tip growth directions are labelled by red arrows, and
988 directions of nodule apex were indicated by yellow arrows. VB, vascular bundle.

989 (C-E) WT and *Gmpin1abc* mutants were transformed by *Gmpin9d-RNAi* construct (with
990 dTomato-tag). The positive hairy roots were selected based on fluorescence and further
991 infected by *BXYD3*, and the profile of nodule diameter was tracked in D (n=613, 618, 624) at
992 14dpi. Expression level of *GmPIN9d* was detected by RT-qPCR (E, n=4), *Gmactin11* was used
993 as the normalization gene (E).

994 (F) Model for polar auxin transport in nodule primordium and developing nodule. Stage I,
995 GmPIN1 mainly directs auxin flow to the outer cortical cells, and partial auxin flows away
996 from outer cortical cells. Stage II and III: GmPIN1-dependent auxin stream flows towards the
997 nodule primordium, and some auxin is retrieved to the neighboring cells. Stage IV: auxin
998 stream is transported within vascular bundles towards nodule via GmPIN1 and GmPIN9d-

999 dependent polar auxin transport. Auxin accumulation is depicted in green, auxin gradient is
1000 indicated in light green, and the presumptive routes of auxin flow are depicted by arrows (red
1001 arrows: GmPIN1-mediation; purple arrows: GmPIN9d-mediation). Flavonoid and cytokinin
1002 act as the elicitors to mediate rapid auxin stream redirection.
1003 Scale bars, 100 μ m (B), 1cm (C). Error bar=S.D.

1004

1005

1006

1007

1008 References

1009

1010 **Abas, L., Kolb, M., Stadlmann, J., Janacek, D.P., Lukic, K., Schwechheimer, C., Sazanov, L.A.,**
1011 **Mach, L., Friml, J., and Hammes, U.Z.** (2021). Naphthylphthalamic acid associates with
1012 and inhibits PIN auxin transporters. *Proc Natl Acad Sci U S A* **118**.

1013 **Adamowski, M., and Friml, J.** (2015). PIN-dependent auxin transport: action, regulation, and
1014 evolution. *Plant Cell* **27**, 20-32.

1015 **Bai, M., Yuan, J., Kuang, H., Gong, P., Li, S., Zhang, Z., Liu, B., Sun, J., Yang, M., Yang, L., Wang,**
1016 **D., Song, S., and Guan, Y.** (2020). Generation of a multiplex mutagenesis population
1017 via pooled CRISPR-Cas9 in soya bean. *Plant Biotechnol J* **18**, 721-731.

1018 **Bailey, T.L., Boden, M., Buske, F.A., Frith, M., Grant, C.E., Clementi, L., Ren, J., Li, W.W., and**
1019 **Noble, W.S.** (2009). MEME SUITE: tools for motif discovery and searching. *Nucleic*
1020 *Acids Res* **37**, W202-208.

1021 **Benkova, E., and Bielach, A.** (2010). Lateral root organogenesis - from cell to organ. *Curr Opin*
1022 *Plant Biol* **13**, 677-683.

1023 **Benkova, E., Michniewicz, M., Sauer, M., Teichmann, T., Seifertova, D., Jurgens, G., and**
1024 **Friml, J.** (2003). Local, efflux-dependent auxin gradients as a common module for
1025 plant organ formation. *Cell* **115**, 591-602.

1026 **Bozsoki, Z., Gysel, K., Hansen, S.B., Lironi, D., Kronauer, C., Feng, F., de Jong, N., Vinther, M.,**
1027 **Kamble, M., Thygesen, M.B., Engholm, E., Kofoed, C., Fort, S., Sullivan, J.T., Ronson,**
1028 **C.W., Jensen, K.J., Blaise, M., Oldroyd, G., Stougaard, J., Andersen, K.R., and**
1029 **Radutoiu, S.** (2020). Ligand-recognizing motifs in plant LysM receptors are major
1030 determinants of specificity. *Science* **369**, 663-670.

1031 **Brown, D.E., Rashotte, A.M., Murphy, A.S., Normanly, J., Tague, B.W., Peer, W.A., Taiz, L.,**
1032 **and Muday, G.K.** (2001). Flavonoids act as negative regulators of auxin transport in
1033 vivo in arabidopsis. *Plant Physiol* **126**, 524-535.

1034 **Buer, C.S., Kordbacheh, F., Truong, T.T., Hocart, C.H., and Djordjevic, M.A.** (2013). Alteration
1035 of flavonoid accumulation patterns in transparent testa mutants disturbs auxin
1036 transport, gravity responses, and imparts long-term effects on root and shoot
1037 architecture. *Planta* **238**, 171-189.

1038 **Cai, Z., Wang, Y., Zhu, L., Tian, Y., Chen, L., Sun, Z., Ullah, I., and Li, X.** (2017).
1039 GmTIR1/GmAFB3-based auxin perception regulated by miR393 modulates soybean
1040 nodulation. *New Phytol* **215**, 672-686.

1041 **Calvert, H.E., Pence, M.K., Pierce, M., Malik, N.S.A., and Bauer, W.D.** (1984). Anatomical
1042 analysis of the development and distribution of Rhizobium infections in soybean roots.
1043 *Canadian Journal of Botany* **62**, 2375-2384.

1044 **Chen, X., Irani, N.G., and Friml, J.** (2011). Clathrin-mediated endocytosis: the gateway into
1045 plant cells. *Curr Opin Plant Biol* **14**, 674-682.

1046 **Du, M., Spalding, E.P., and Gray, W.M.** (2020). Rapid Auxin-Mediated Cell Expansion. *Annu*
1047 *Rev Plant Biol* **71**, 379-402.

1048 **Feraru, E., and Friml, J.** (2008). PIN polar targeting. *Plant Physiol* **147**, 1553-1559.

1049 **Friml, J., Wisniewska, J., Benkova, E., Mendgen, K., and Palme, K.** (2002). Lateral relocation
1050 of auxin efflux regulator PIN3 mediates tropism in Arabidopsis. *Nature* **415**, 806-809.

1051 **Galweiler, L., Guan, C., Muller, A., Wisman, E., Mendgen, K., Yephremov, A., and Palme, K.**
1052 (1998). Regulation of polar auxin transport by AtPIN1 in Arabidopsis vascular tissue.
1053 *Science* **282**, 2226-2230.

- 1054 **Gauthier-Coles, C., White, R.G., and Mathesius, U.** (2018). Nodulating Legumes Are
1055 Distinguished by a Sensitivity to Cytokinin in the Root Cortex Leading to Pseudonodule
1056 Development. *Front Plant Sci* **9**, 1901.
- 1057 **Geldner, N., Anders, N., Wolters, H., Keicher, J., Kornberger, W., Muller, P., Delbarre, A.,**
1058 **Ueda, T., Nakano, A., and Jurgens, G.** (2003). The Arabidopsis GNOM ARF-GEF
1059 mediates endosomal recycling, auxin transport, and auxin-dependent plant growth.
1060 *Cell* **112**, 219-230.
- 1061 **Hirsch, A.M., Bhuvaneswari, T.V., Torrey, J.G., and Bisseling, T.** (1989). Early nodulin genes
1062 are induced in alfalfa root outgrowths elicited by auxin transport inhibitors. *Proc Natl*
1063 *Acad Sci U S A* **86**, 1244-1248.
- 1064 **Ip, H., D'Aoust, F., Begum, A.A., Zhang, H., Smith, D.L., Driscoll, B.T., and Charles, T.C.** (2001).
1065 *Bradyrhizobium japonicum* mutants with enhanced sensitivity to genistein resulting in
1066 altered nod gene regulation. *Mol Plant Microbe Interact* **14**, 1404-1410.
- 1067 **Kereszt, A., Li, D., Indrasumunar, A., Nguyen, C.D., Nontachaiyapoom, S., Kinkema, M., and**
1068 **Gresshoff, P.M.** (2007). *Agrobacterium rhizogenes*-mediated transformation of
1069 soybean to study root biology. *Nat Protoc* **2**, 948-952.
- 1070 **Kohlen, W., Ng, J.L.P., Deinum, E.E., and Mathesius, U.** (2018). Auxin transport, metabolism,
1071 and signalling during nodule initiation: indeterminate and determinate nodules. *J Exp*
1072 *Bot* **69**, 229-244.
- 1073 **Kuhn, B.M., Nodzynski, T., Errafi, S., Bucher, R., Gupta, S., Aryal, B., Dobrev, P., Bigler, L.,**
1074 **Geisler, M., Zazimalova, E., Friml, J., and Ringli, C.** (2017). Flavonol-induced changes
1075 in PIN2 polarity and auxin transport in the Arabidopsis thaliana rol1-2 mutant require
1076 phosphatase activity. *Sci Rep* **7**, 41906.
- 1077 **Kumar, S., Stecher, G., Li, M., Knyaz, C., and Tamura, K.** (2018). MEGA X: Molecular
1078 Evolutionary Genetics Analysis across Computing Platforms. *Mol Biol Evol* **35**, 1547-
1079 1549.
- 1080 **Kurepa, J., Shull, T.E., and Smalle, J.A.** (2019). Antagonistic activity of auxin and cytokinin in
1081 shoot and root organs. *Plant Direct* **3**, e00121.
- 1082 **Laffont, C., Ivanovici, A., Gautrat, P., Brault, M., Djordjevic, M.A., and Frugier, F.** (2020). The
1083 NIN transcription factor coordinates CEP and CLE signaling peptides that regulate
1084 nodulation antagonistically. *Nat Commun* **11**, 3167.
- 1085 **Lang, K., Lindemann, A., Hauser, F., and Gottfert, M.** (2008). The genistein stimulon of
1086 *Bradyrhizobium japonicum*. *Mol Genet Genomics* **279**, 203-211.
- 1087 **Larkin, M.A., Blackshields, G., Brown, N.P., Chenna, R., McGettigan, P.A., McWilliam, H.,**
1088 **Valentin, F., Wallace, I.M., Wilm, A., Lopez, R., Thompson, J.D., Gibson, T.J., and**
1089 **Higgins, D.G.** (2007). Clustal W and Clustal X version 2.0. *Bioinformatics* **23**, 2947-2948.
- 1090 **Lewis, D.R., and Muday, G.K.** (2009). Measurement of auxin transport in Arabidopsis thaliana.
1091 *Nat Protoc* **4**, 437-451.
- 1092 **Liao, C.Y., Smet, W., Brunoud, G., Yoshida, S., Vernoux, T., and Weijers, D.** (2015). Reporters
1093 for sensitive and quantitative measurement of auxin response. *Nat Methods* **12**, 207-
1094 210, 202 p following 210.
- 1095 **Liu, C.W., and Murray, J.D.** (2016). The Role of Flavonoids in Nodulation Host-Range
1096 Specificity: An Update. *Plants (Basel)* **5**, 33.
- 1097 **Livingston, D., Tuong, T., Nogueira, M., and Sinclair, T.** (2019). Three-dimensional
1098 reconstruction of soybean nodules provides an update on vascular structure. *Am J Bot*
1099 **106**, 507-513.

- 1100 **Marhavy, P., Duclercq, J., Weller, B., Feraru, E., Bielach, A., Offringa, R., Friml, J.,**
1101 **Schwechheimer, C., Murphy, A., and Benkova, E.** (2014). Cytokinin controls polarity
1102 of PIN1-dependent auxin transport during lateral root organogenesis. *Curr Biol* **24**,
1103 1031-1037.
- 1104 **Mashiguchi, K., Tanaka, K., Sakai, T., Sugawara, S., Kawaide, H., Natsume, M., Hanada, A.,**
1105 **Yaeno, T., Shirasu, K., Yao, H., McSteen, P., Zhao, Y., Hayashi, K., Kamiya, Y., and**
1106 **Kasahara, H.** (2011). The main auxin biosynthesis pathway in Arabidopsis. *Proc Natl*
1107 *Acad Sci U S A* **108**, 18512-18517.
- 1108 **Mathesius, U., Schlaman, H.R., Spaink, H.P., Of Sautter, C., Rolfe, B.G., and Djordjevic, M.A.**
1109 (1998). Auxin transport inhibition precedes root nodule formation in white clover
1110 roots and is regulated by flavonoids and derivatives of chitin oligosaccharides. *The*
1111 *Plant journal : for cell and molecular biology* **14**, 23-34.
- 1112 **Mravec, J., Kubes, M., Bielach, A., Gaykova, V., Petrasek, J., Skupa, P., Chand, S., Benkova,**
1113 **E., Zazimalova, E., and Friml, J.** (2008). Interaction of PIN and PGP transport
1114 mechanisms in auxin distribution-dependent development. *Development* **135**, 3345-
1115 3354.
- 1116 **Muller, A., Guan, C., Galweiler, L., Tanzler, P., Huijser, P., Marchant, A., Parry, G., Bennett,**
1117 **M., Wisman, E., and Palme, K.** (1998). AtPIN2 defines a locus of Arabidopsis for root
1118 gravitropism control. *EMBO J* **17**, 6903-6911.
- 1119 **Murray, J.D., Karas, B.J., Sato, S., Tabata, S., Amyot, L., and Szczyglowski, K.** (2007). A
1120 cytokinin perception mutant colonized by Rhizobium in the absence of nodule
1121 organogenesis. *Science* **315**, 101-104.
- 1122 **Ng, J.L., Hassan, S., Truong, T.T., Hocart, C.H., Laffont, C., Frugier, F., and Mathesius, U.**
1123 (2015). Flavonoids and Auxin Transport Inhibitors Rescue Symbiotic Nodulation in the
1124 *Medicago truncatula* Cytokinin Perception Mutant cre1. *Plant Cell* **27**, 2210-2226.
- 1125 **Ng, J.L.P., and Mathesius, U.** (2018). Acropetal Auxin Transport Inhibition Is Involved in
1126 Indeterminate But Not Determinate Nodule Formation. *Front Plant Sci* **9**, 169.
- 1127 **Okada, K., Ueda, J., Komaki, M.K., Bell, C.J., and Shimura, Y.** (1991). Requirement of the
1128 Auxin Polar Transport System in Early Stages of Arabidopsis Floral Bud Formation.
1129 *Plant Cell* **3**, 677-684.
- 1130 **Pacios-Bras, C., Schlaman, H.R., Boot, K., Admiraal, P., Langerak, J.M., Stougaard, J., and**
1131 **Spaink, H.P.** (2003). Auxin distribution in *Lotus japonicus* during root nodule
1132 development. *Plant Mol Biol* **52**, 1169-1180.
- 1133 **Peer, W.A., Bandyopadhyay, A., Blakeslee, J.J., Makam, S.N., Chen, R.J., Masson, P.H., and**
1134 **Murphy, A.S.** (2004). Variation in expression and protein localization of the PIN family
1135 of auxin efflux facilitator proteins in flavonoid mutants with altered auxin transport in
1136 *Arabidopsis thaliana*. *Plant Cell* **16**, 1898-1911.
- 1137 **Petrasek, J., Mravec, J., Bouchard, R., Blakeslee, J.J., Abas, M., Seifertova, D., Wisniewska,**
1138 **J., Tadele, Z., Kubes, M., Covanova, M., Dhonukshe, P., Skupa, P., Benkova, E., Perry,**
1139 **L., Krecek, P., Lee, O.R., Fink, G.R., Geisler, M., Murphy, A.S., Luschnig, C., Zazimalova,**
1140 **E., and Friml, J.** (2006). PIN proteins perform a rate-limiting function in cellular auxin
1141 efflux. *Science* **312**, 914-918.
- 1142 **Pierre-Jerome, E., Drapek, C., and Benfey, P.N.** (2018). Regulation of Division and
1143 Differentiation of Plant Stem Cells. *Annu Rev Cell Dev Biol* **34**, 289-310.
- 1144 **Popp, C., and Ott, T.** (2011). Regulation of signal transduction and bacterial infection during
1145 root nodule symbiosis. *Curr Opin Plant Biol* **14**, 458-467.

- 1146 **Qi, J., Wang, Y., Yu, T., Cunha, A., Wu, B., Vernoux, T., Meyerowitz, E., and Jiao, Y.** (2014).
1147 Auxin depletion from leaf primordia contributes to organ patterning. *Proc Natl Acad*
1148 *Sci U S A* **111**, 18769-18774.
- 1149 **Reid, D., Nadzieja, M., Novak, O., Heckmann, A.B., Sandal, N., and Stougaard, J.** (2017).
1150 Cytokinin Biosynthesis Promotes Cortical Cell Responses during Nodule Development.
1151 *Plant Physiol* **175**, 361-375.
- 1152 **Rightmyer, A.P., and Long, S.R.** (2011). Pseudonodule formation by wild-type and symbiotic
1153 mutant *Medicago truncatula* in response to auxin transport inhibitors. *Mol Plant*
1154 *Microbe Interact* **24**, 1372-1384.
- 1155 **Santelia, D., Henrichs, S., Vincenzetti, V., Sauer, M., Bigler, L., Klein, M., Bailly, A., Lee, Y.,**
1156 **Friml, J., Geisler, M., and Martinoia, E.** (2008). Flavonoids redirect PIN-mediated polar
1157 auxin fluxes during root gravitropic responses. *J Biol Chem* **283**, 31218-31226.
- 1158 **Schaller, G.E., Bishopp, A., and Kieber, J.J.** (2015). The yin-yang of hormones: cytokinin and
1159 auxin interactions in plant development. *Plant Cell* **27**, 44-63.
- 1160 **Schiessl, K., Lilley, J.L.S., Lee, T., Tamvakis, I., Kohlen, W., Bailey, P.C., Thomas, A., Luptak,**
1161 **J., Ramakrishnan, K., Carpenter, M.D., Mysore, K.S., Wen, J., Ahnert, S., Grieneisen,**
1162 **V.A., and Oldroyd, G.E.D.** (2019). NODULE INCEPTION Recruits the Lateral Root
1163 Developmental Program for Symbiotic Nodule Organogenesis in *Medicago truncatula*.
1164 *Curr Biol* **29**, 3657-3668 e3655.
- 1165 **Stepanova, A.N., Yun, J., Robles, L.M., Novak, O., He, W., Guo, H., Ljung, K., and Alonso, J.M.**
1166 (2011). The Arabidopsis YUCCA1 flavin monooxygenase functions in the indole-3-
1167 pyruvic acid branch of auxin biosynthesis. *Plant Cell* **23**, 3961-3973.
- 1168 **Subramanian, S., Stacey, G., and Yu, O.** (2006). Endogenous isoflavones are essential for the
1169 establishment of symbiosis between soybean and *Bradyrhizobium japonicum*. *The*
1170 *Plant journal : for cell and molecular biology* **48**, 261-273.
- 1171 **Subramanian, S., Stacey, G., and Yu, O.** (2007). Distinct, crucial roles of flavonoids during
1172 legume nodulation. *Trends Plant Sci* **12**, 282-285.
- 1173 **Suzuki, T., and Kawaguchi, M.** (2014). Root nodulation: a developmental program involving
1174 cell fate conversion triggered by symbiotic bacterial infection. *Curr Opin Plant Biol* **21**,
1175 16-22.
- 1176 **Suzuki, T., Yano, K., Ito, M., Umehara, Y., Suganuma, N., and Kawaguchi, M.** (2012). Positive
1177 and negative regulation of cortical cell division during root nodule development in
1178 *Lotus japonicus* is accompanied by auxin response. *Development* **139**, 3997-4006.
- 1179 **Teale, W.D., Pasternak, T., Dal Bosco, C., Dovzhenko, A., Kratzat, K., Bildl, W., Schworer, M.,**
1180 **Falk, T., Ruperti, B., Schaefer, J.V., Shahriari, M., Pilgermayer, L., Li, X., Lubben, F.,**
1181 **Pluckthun, A., Schulte, U., and Palme, K.** (2021). Flavonol-mediated stabilization of
1182 PIN efflux complexes regulates polar auxin transport. *EMBO J* **40**, e104416.
- 1183 **Turner, M., Nizampatnam, N.R., Baron, M., Coppin, S., Damodaran, S., Adhikari, S.,**
1184 **Arunachalam, S.P., Yu, O., and Subramanian, S.** (2013). Ectopic expression of miR160
1185 results in auxin hypersensitivity, cytokinin hyposensitivity, and inhibition of symbiotic
1186 nodule development in soybean. *Plant Physiol* **162**, 2042-2055.
- 1187 **Ulmasov, T., Murfett, J., Hagen, G., and Guilfoyle, T.J.** (1997). Aux/IAA proteins repress
1188 expression of reporter genes containing natural and highly active synthetic auxin
1189 response elements. *Plant Cell* **9**, 1963-1971.
- 1190 **van Noorden, G.E., Kerim, T., Goffard, N., Wiblin, R., Pellerone, F.I., Rolfe, B.G., and**
1191 **Mathesius, U.** (2007). Overlap of proteome changes in *Medicago truncatula* in
1192 response to auxin and *Sinorhizobium meliloti*. *Plant Physiol* **144**, 1115-1131.

- 1193 **Viaene, T., Delwiche, C.F., Rensing, S.A., and Friml, J.** (2013). Origin and evolution of PIN
1194 auxin transporters in the green lineage. *Trends Plant Sci* **18**, 5-10.
- 1195 **Wang, Y., Chai, C., Valliyodan, B., Maupin, C., Annen, B., and Nguyen, H.T.** (2015a). Genome-
1196 wide analysis and expression profiling of the PIN auxin transporter gene family in
1197 soybean (*Glycine max*). *BMC Genomics* **16**, 951.
- 1198 **Wang, Y., Yang, W., Zuo, Y., Zhu, L., Hastwell, A.H., Chen, L., Tian, Y., Su, C., Ferguson, B.J.,
1199 and Li, X.** (2019). GmYUC2a mediates auxin biosynthesis during root development and
1200 nodulation in soybean. *J Exp Bot* **70**, 3165-3176.
- 1201 **Wang, Y., Li, K., Chen, L., Zou, Y., Liu, H., Tian, Y., Li, D., Wang, R., Zhao, F., Ferguson, B.J.,
1202 Gresshoff, P.M., and Li, X.** (2015b). MicroRNA167-Directed Regulation of the Auxin
1203 Response Factors GmARF8a and GmARF8b Is Required for Soybean Nodulation and
1204 Lateral Root Development. *Plant Physiol* **168**, 984-999.
- 1205 **Weijers, D., Sauer, M., Meurette, O., Friml, J., Ljung, K., Sandberg, G., Hooykaas, P., and
1206 Offringa, R.** (2005). Maintenance of embryonic auxin distribution for apical-basal
1207 patterning by PIN-FORMED-dependent auxin transport in *Arabidopsis*. *Plant Cell* **17**,
1208 2517-2526.
- 1209 **Wisniewska, J., Xu, J., Seifertova, D., Brewer, P.B., Ruzicka, K., Blilou, I., Rouquie, D.,
1210 Benkova, E., Scheres, B., and Friml, J.** (2006). Polar PIN localization directs auxin flow
1211 in plants. *Science* **312**, 883.
- 1212 **Wu, C., Dickstein, R., Cary, A.J., and Norris, J.H.** (1996). The Auxin Transport Inhibitor N-(1-
1213 Naphthyl)phthalamic Acid Elicits Pseudonodules on Nonnodulating Mutants of White
1214 Sweetclover. *Plant Physiol* **110**, 501-510.
- 1215 **Wu, M.F., Yamaguchi, N., Xiao, J., Bargmann, B., Estelle, M., Sang, Y., and Wagner, D.** (2015).
1216 Auxin-regulated chromatin switch directs acquisition of flower primordium founder
1217 fate. *Elife* **4**, e09269.
- 1218 **Xiao, T.T., Schilderink, S., Moling, S., Deinum, E.E., Kondorosi, E., Franssen, H., Kulikova, O.,
1219 Niebel, A., and Bisseling, T.** (2014). Fate map of *Medicago truncatula* root nodules.
1220 *Development* **141**, 3517-3528.
- 1221 **Xiong, Y., and Jiao, Y.** (2019). The Diverse Roles of Auxin in Regulating Leaf Development.
1222 *Plants (Basel)* **8**, 243.
- 1223 **Xu, J., and Scheres, B.** (2005). Dissection of *Arabidopsis* ADP-RIBOSYLATION FACTOR 1
1224 function in epidermal cell polarity. *Plant Cell* **17**, 525-536.
- 1225 **Yamaguchi, N., Wu, M.F., Winter, C.M., Berns, M.C., Nole-Wilson, S., Yamaguchi, A.,
1226 Coupland, G., Krizek, B.A., and Wagner, D.** (2013). A molecular framework for auxin-
1227 mediated initiation of flower primordia. *Dev Cell* **24**, 271-282.
- 1228 **Yang, H., Wang, Y., Li, L., Li, F., He, Y., Wu, J., and Wei, C.** (2019). Transcriptomic and
1229 Phytochemical Analyses Reveal Root-Mediated Resource-Based Defense Response to
1230 Leaf Herbivory by *Ectropis oblique* in Tea Plant (*Camellia sinensis*). *J Agric Food Chem*
1231 **67**, 5465-5476.
- 1232 **Zhang, J., Subramanian, S., Stacey, G., and Yu, O.** (2009). Flavones and flavonols play distinct
1233 critical roles during nodulation of *Medicago truncatula* by *Sinorhizobium meliloti*. *The
1234 Plant journal : for cell and molecular biology* **57**, 171-183.
- 1235 **Zhang, J., Nodzynski, T., Pencik, A., Rolcik, J., and Friml, J.** (2010). PIN phosphorylation is
1236 sufficient to mediate PIN polarity and direct auxin transport. *Proc Natl Acad Sci U S A*
1237 **107**, 918-922.
- 1238 **Zhang, X., Huang, X., Li, Y., Tao, F., Zhao, Q., and Li, W.** (2021). Polar auxin transport May Be
1239 responsive to specific features of flavonoid structure. *Phytochemistry* **185**, 112702.

1240 **Zhao, Y.** (2018). Essential Roles of Local Auxin Biosynthesis in Plant Development and in
1241 Adaptation to Environmental Changes. *Annu Rev Plant Biol* **69**, 417-435.
1242

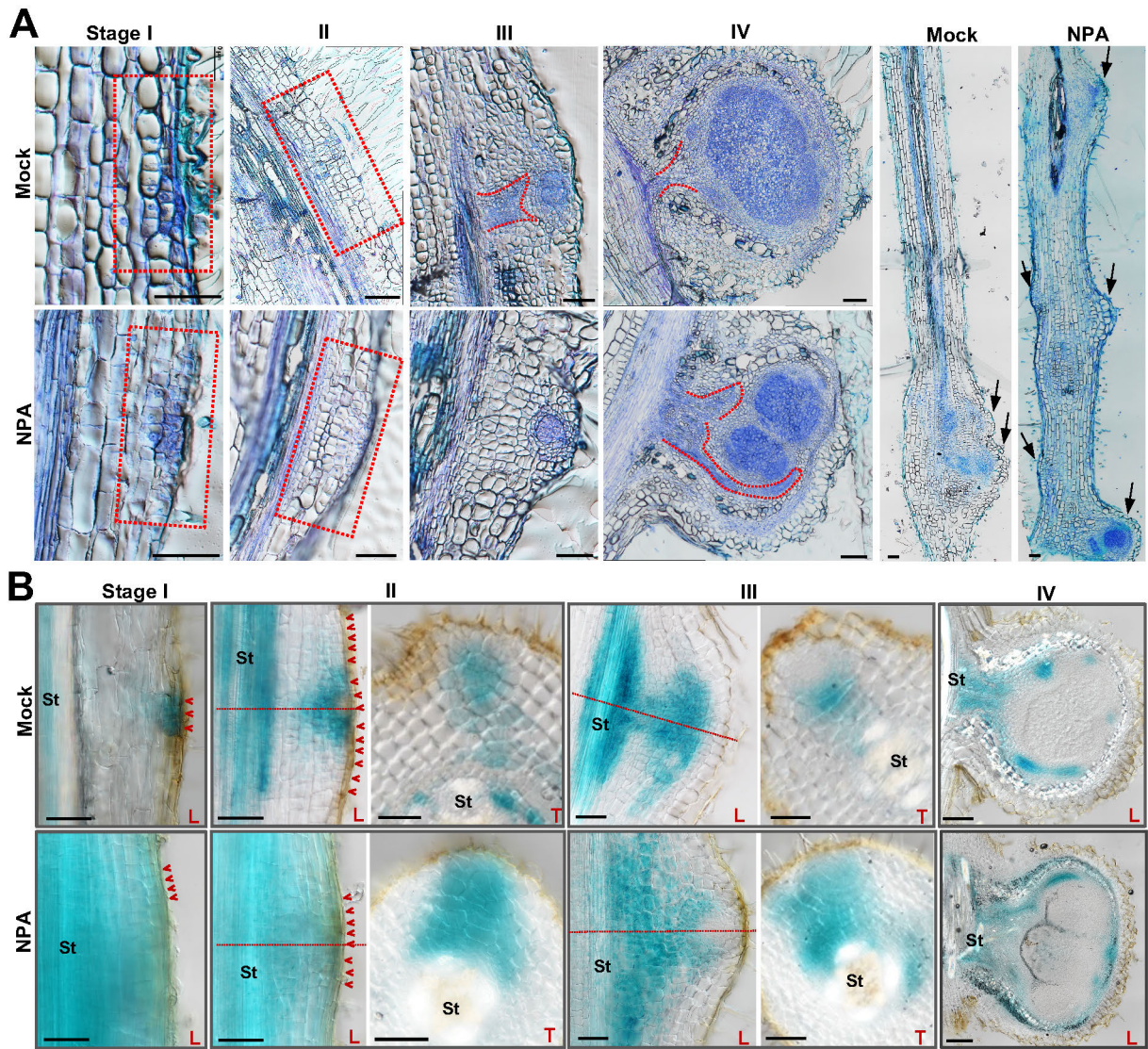


Figure 1. NPA disrupts auxin distribution and nodule formation.

(A-B) 7-day-old WT (A) or *DR5-V2-GUS* transgenic soybean plants (B) were infected by *BXYD3*, and then incubated in low-nitrogen hydroponic solution containing 10^{-7} M NPA or DMSO (as mock control). Root-shoot junction area were collected in series at 4dpi till 14dpi for resin embedding and sectioning. The morphology of soybean nodules in stage I to IV was sectioned in longitudinal direction (A). Red boxes label the primordium area, dotted lines label the vascular bundles, and black arrows highlight nodule or nodule primordium (A). *DR5-V2* activity in different nodule stages was stained and captured by sectioning in longitudinal (L) or transversal (T) direction (B). St: root stele. Red dot lines label the sectioning areas in transversal direction. Red arrows highlight the dividing cortical cells. Scale bars, 100 µm (A, B).

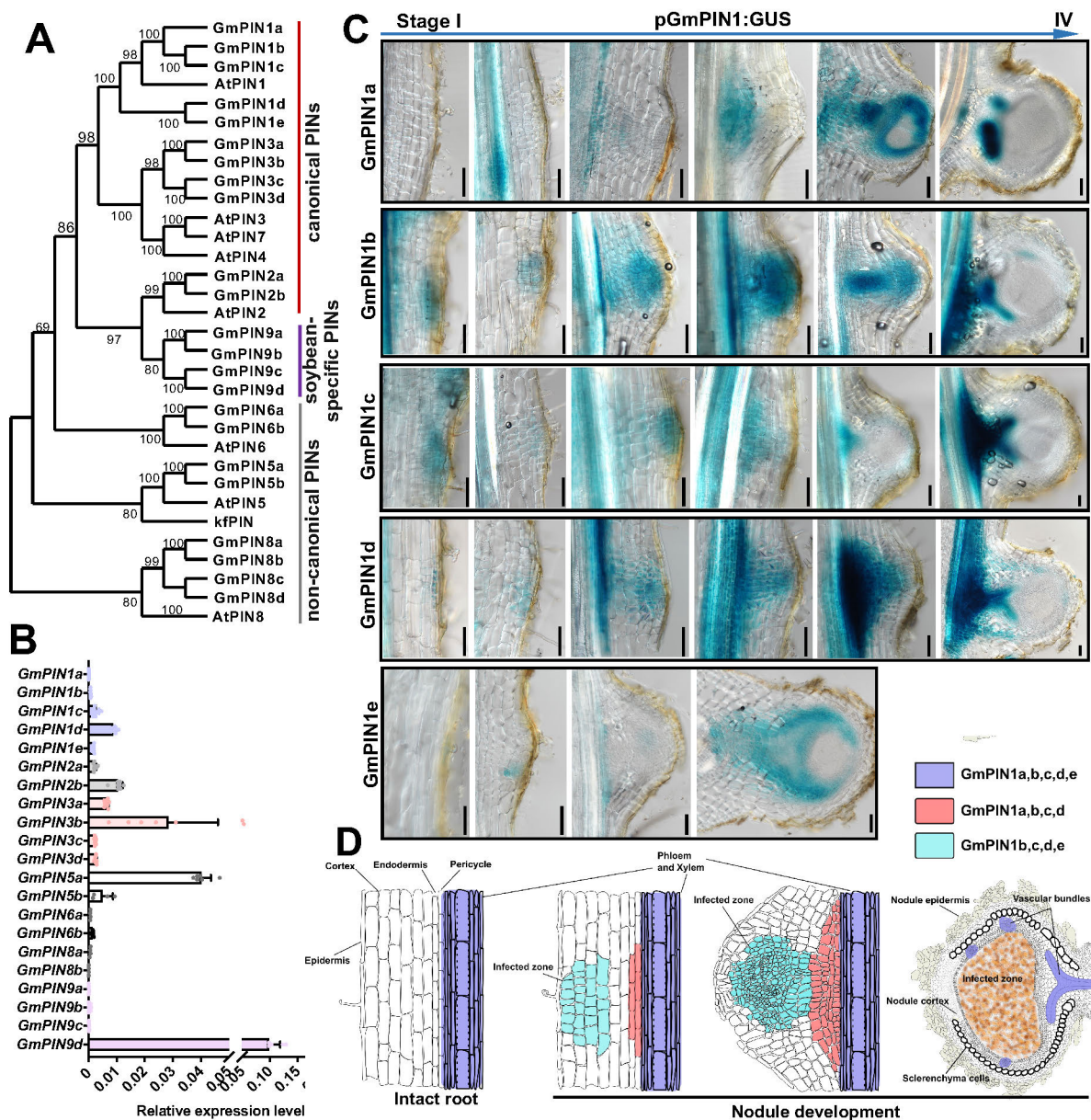


Figure 2. Expression pattern of *GmPINs* during nodule development.

(A) The phylogenetic tree of PIN proteins from *Arabidopsis* (At), *Glycine max* (Gm) and *Klebsormidium flaccidum* (Kf) was constructed using MEGA X. These PIN genes were grouped as canonical, non-canonical and soybean-specific PIN types.

(B) Transcript level of 23 *GmPIN* genes was detected by RT-qPCR in nodules at 14dpi ($n \geq 3$), *Gmactin11* was the normalization gene.

(C) *pGmPIN1a, b, c, d, e::GUS* constructs were introduced in WT soybean plants by hairy root transformation, the positive roots were infected by *BXYD3*. Root segments were collected at 4dpi till 14dpi. Root sectioning was performed for the further histochemical staining.

(D) Cartoon model represents the spatial and temporal expression pattern (different colors) of *GmPIN1s* during nodule development.

Scale bars, 100 μm (C). Error bar=S.D.

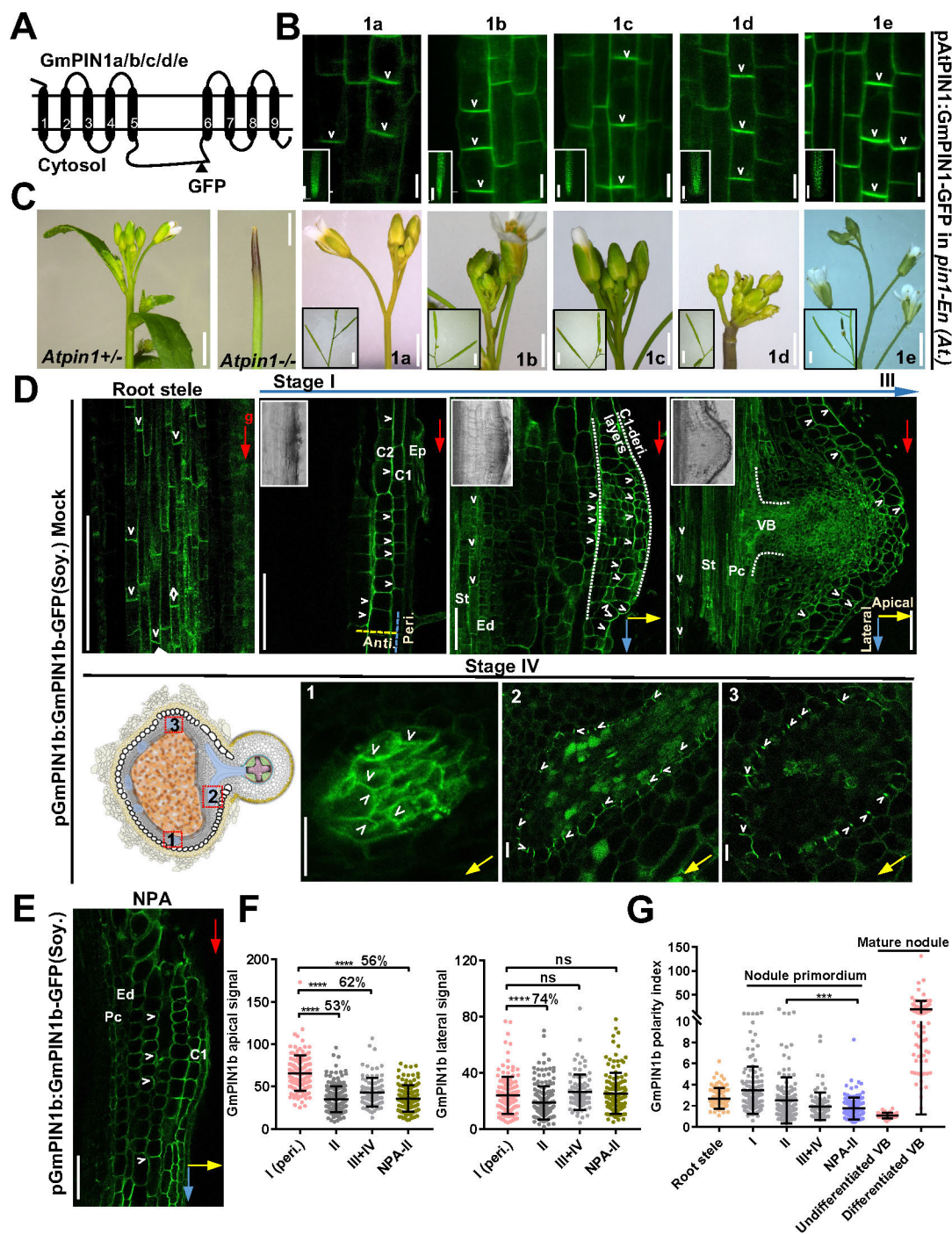


Figure 3. GmPIN1 are localization conserved with AtPIN1 and direct auxin flow during nodule primordium formation.

(A) Predicted topology of GmPIN1 proteins. The following GmPIN1-GFP constructs were established based on the insertion position of GFP in the hydrophilic loop.

(B-C) GmPIN1a-e distribution and polarity were visualized in roots of the transgenic *Arabidopsis* plants (*pAtPIN1: GmPIN1-GFP* in *pin1-En Arabidopsis* (*At*.) mutant background (B, C). The phenotypes of inflorescence and silique (inset boxes) were shown in C. Polar localization of GmPIN1 in the basal side of PM in root stele (inset boxes) was highlighted by white arrows (B).

(D) GmPIN1b localization was visualized in roots and different stages of nodules in the transgenic soybean plant *pGmPIN1b:GmPIN1b-GFP*. The polarity of GmPIN1b (with predominant polarity toward nodule apex) was highlighted by white arrows. Dot lines label the area of C1-derived cell layers or vascular bundle. Pictures with bright field view were shown in the inset boxes of upper panels. The images in lower panels showed the enlarged views of boxed areas in the representative cartoon (1: undifferentiated vascular bundles; 2 and 3: differentiated vascular bundles). Yellow and blue dot lines represent GmPIN1b signal on periclinal and anticlinal directions at stage I.

(E) GmPIN1b localization was visualized in nodule primordium (stage II) of NPA (10^{-7} M, 4days)-treated *pGmPIN1b:GmPIN1b-GFP* seedlings. White arrows label GmPIN1b polarity toward nodule apex.

(F-G) GmPIN1b signal toward nodule apex (apical) or perpendicular to nodule apex (lateral) was individually measured in F (n=136, 189, 89, 129, 136, 189, 89, 129). The comparison ratio of GmPIN1b signal in different nodule primordium stage relative to those in stage I was shown as percentage in F. Polar index of GmPIN1b was quantified by calculation of GmPIN1b signal ratio of apical-targeted GmPIN1b signals relative to them in the lateral sides (G: n=90, 136, 189, 89, 129, 40, 102).

Scale bars, 5 μ m (B), 50 μ m (B, inset box), 5mm (C), 100 μ m (D upper panel, E), 20 μ m (D lower panel). Error bar=S.D. In D-E: Ep, epidermis; C1, 1st cortical cell layer; C2, 2nd cortical cell layer; Ed, endodermis; Pc, pericycle; St, stele; VB, vascular bundle. Root tip growth directions (g) were labelled by red arrows (D, E). Nodule primordium apex (apical-targeted GmPIN1b) was labelled by yellow arrows, and the lateral localization (perpendicular to the apical direction) of GmPIN1b was labelled by blue arrows (D, E). P-values were determined by two-tailed Student's t-test assuming equal variances (***p<0.001; ****p<0.0001; ns, not significant).

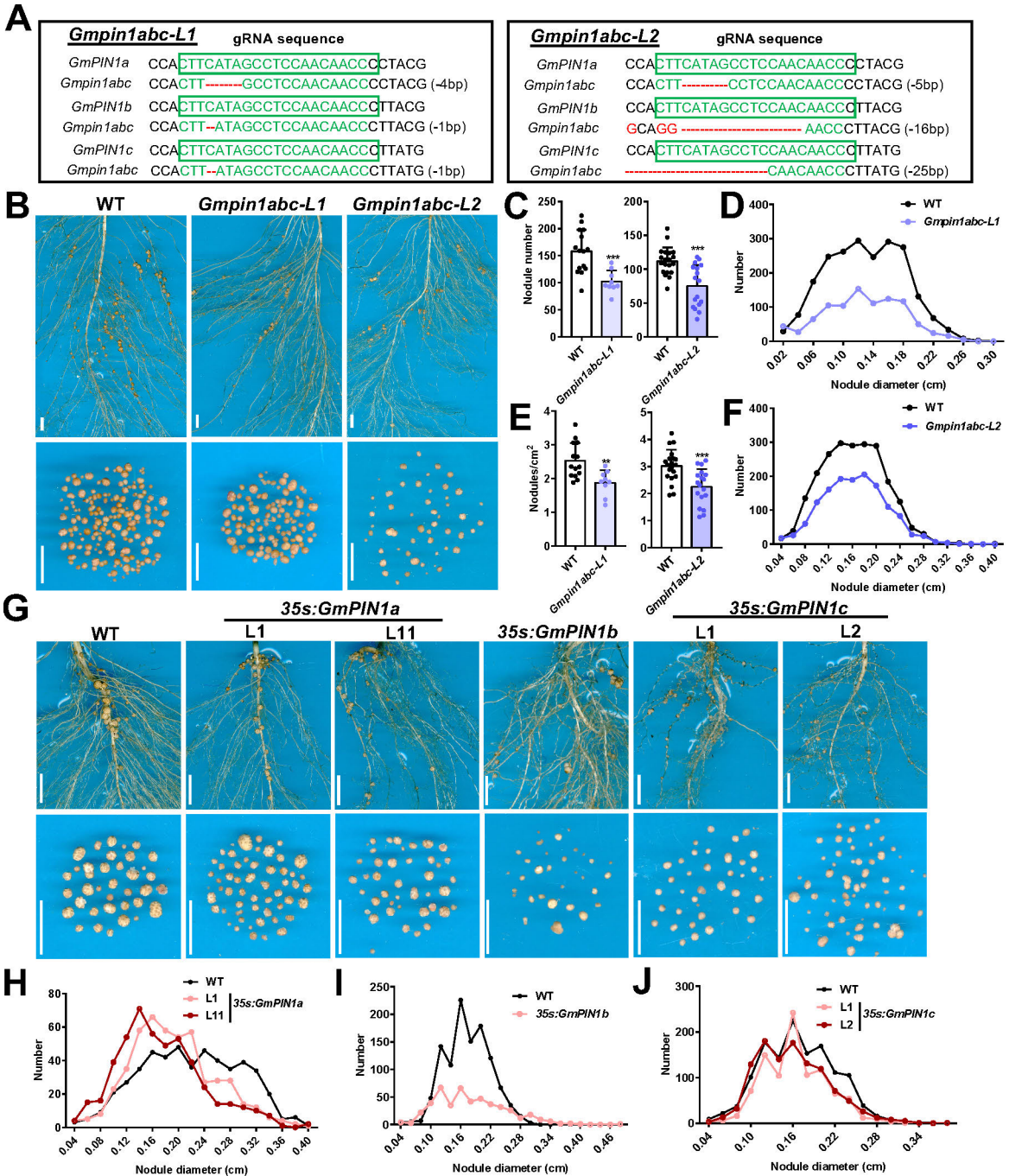


Figure 4. Nodulation phenotypes of *Gmpin1abc* triple mutant and overexpressed *GmPIN1* lines.

(A) *Gmpin1abc* triple mutants were generated via CRISPR-Cas9 gene editing approach. The sequence of *GmPIN1a*, *b*, *c* with the gRNA targeted sites was designed in the first exon of *GmPIN1* genes. gRNA targeted sequences were framed by green, and the mutation or deletion sequences were labelled by red. Two independent triple mutant lines with editing manner were shown.

(B-J) 7-day-old WT, *Gmpin1abc* mutants and *35s:GmPIN1a*, *b* and *c* lines were infected by *BXYD3*, and the nodulation phenotypes were analyzed at 14 dpi. Nodule number (per plant) and density (number per cm²) were quantified in C (n=15, 9, 20, 17) and E (n=15, 9, 20, 17). Profile of nodule diameter was tracked in D (n=2138, 945), F (n=2236, 1404), H (n=848, 930, 480), I (n=1111, 471), J (n=1318, 961, 1096) (all from upper to lower groups).

Scale bars, 1cm (B, G). Error bar=S.D. P-values were determined by two-tailed Student's t-test assuming equal variances (**p< 0.01; ***p< 0.001).

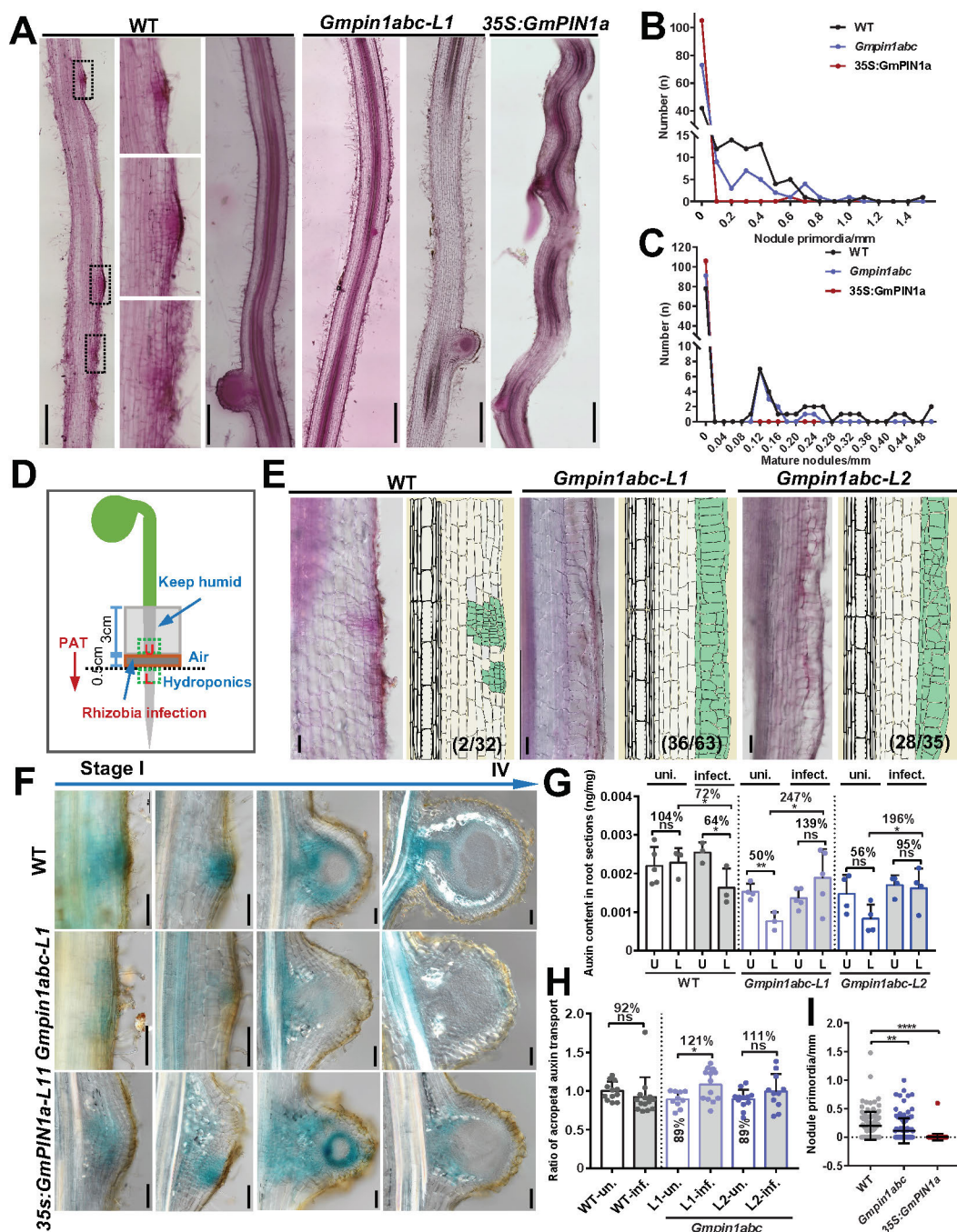


Figure 5. Loss-of-function and gain-of-function of *GmPIN1* both disrupted auxin distribution and nodule primordium initiation.

(A-C, I) 7-day-old WT, *Gmpin1abc-L1* and *35S:GmPIN1a-L11* plants were infected by *BXYD3* for additional 5 days growth. Consistent 1cm root segments were collected from lateral roots at root-shoot junction area. Root segments were sectioned in longitudinal direction and co-stained by chameleon and schiff's fuchsin-sulfite reagents (A). Nodule primordium density and developing nodule density were individually quantified as profile in B ($n=106$) and C ($n=106$). The overall nodule primordium density was analyzed in I ($n=106$). The middle panels of WT in A showed 3 \times enlarged views of boxed areas in the images of left panels.

(D,E-G,H) 0.5cm root segments below root-shoot junction of 5-day-old WT, *Gmpin1abc-L1* and *Gmpin1abc-L2* were performed by 48h continuous *BXYD3* spot inoculation (equipped as the cartoon in D). Auxin content in the upper (U) and lower (L) root segments close to the inoculated position was measured in G (uninfected roots were used as controls) ($n=5, 3, 3, 4, 4, 3, 5, 4, 4, 4, 4$). Polar auxin transport (PAT) efficiency was measured in acropetal direction in H (n=12, 14, 10, 13, 12, 11; red arrow in D labelled PAT direction). The comparison ratio of auxin content in L relative to those in U was shown as percentage in G, and the comparison ratio of auxin transport capacity in infected groups to uninfected groups was shown as percentage in H. Nodule primordium morphology in WT and *Gmpin1abc* mutants was observed at 5dpi after spot inoculation (E). Cartoons simulate cell morphology of each genotype, and green color indicates the dividing cortical cells (E). The percentage in E indicated the proportion of roots with aberrant dividing cortical cells in the total counting roots.

(F) *DR5-V2-GUS* construct was introduced in WT, *Gmpin1abc-L1* and *35S:GmPIN1a-L11* plants by hairy root transformation, and different stages of nodule were collected at 8dpi for sectioning. Auxin distribution was visualized by histochemical GUS staining.

Scale bars, 200 μ m (A), 100 μ m (E, F). Error bar=S.D. P-values were determined by two-tailed Student's t-test assuming equal variances (* $p<0.05$; ** $p<0.01$; **** $p<0.0001$; ns, not significant).

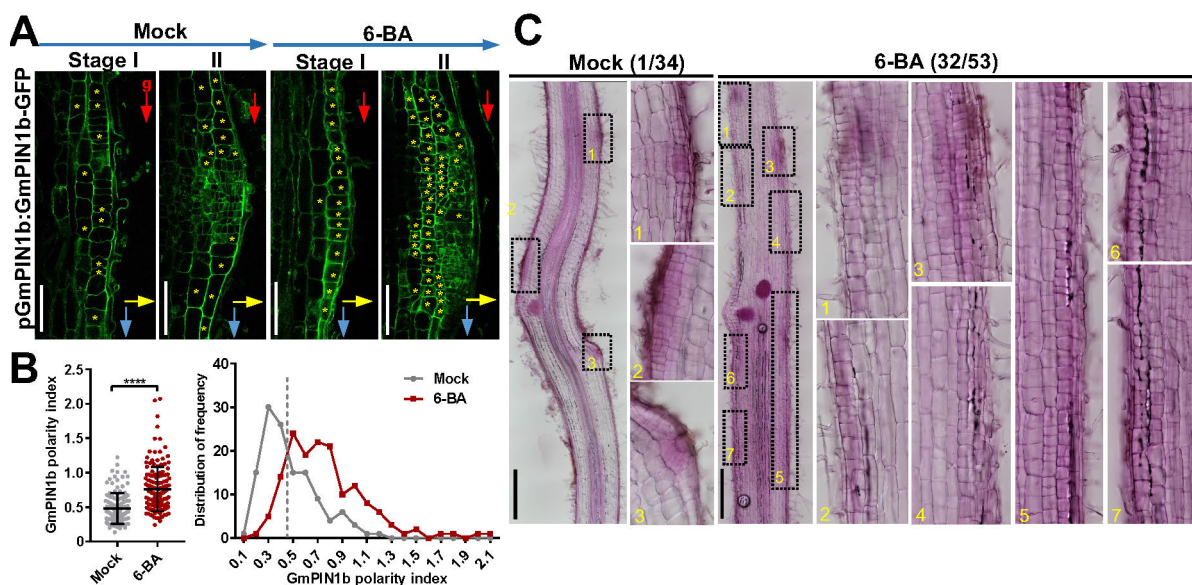


Figure 6. Cytokinin rearranges GmPIN1b polarity.

(A-B) Nodule primordium of *BXYD3*-infected *pGmPIN1b:GmPIN1b-GFP* soybean plants were analyzed at 8dpi (with or without $1\mu\text{M}$ 6-BA treatment for 16h). GmPIN1b-GFP signal in the apical (yellow arrows) and lateral (blue arrows) directions of nodule primordium was calculated and shown as lateral/apical ratio in (B) ($n=126$ from 22 sections, 152 from 36 sections), and the distribution frequency of GmPIN1b signal ratio was shown in the right chart (B, grey dot line marked the cutoff value). The cells with GmPIN1b signal ratio above the cutoff value was highlighted by yellow stars (A). Root tip growth directions (g) were labelled by red arrows (A).

(C) 7-day-old WT plants were infected by *BXYD3*, and then they were irrigated with low-nitrogen hydroponic solution containing $0.1\mu\text{M}$ 6-BA or DMSO (as mock control) for additional 7 days. Cortical root cell morphology was observed by root sectioning. Numbers in the right panels showed 4 \times enlarged views framed in the left image. The percentage indicated the proportion of roots with a cluster of dividing cortical cells in the total counting roots. Scale bars, $100\mu\text{m}$ (A), $500\mu\text{m}$ (C). Error bar=S.D. P-values were determined by two-tailed Student's t-test assuming equal variances (**** $p < 0.0001$).

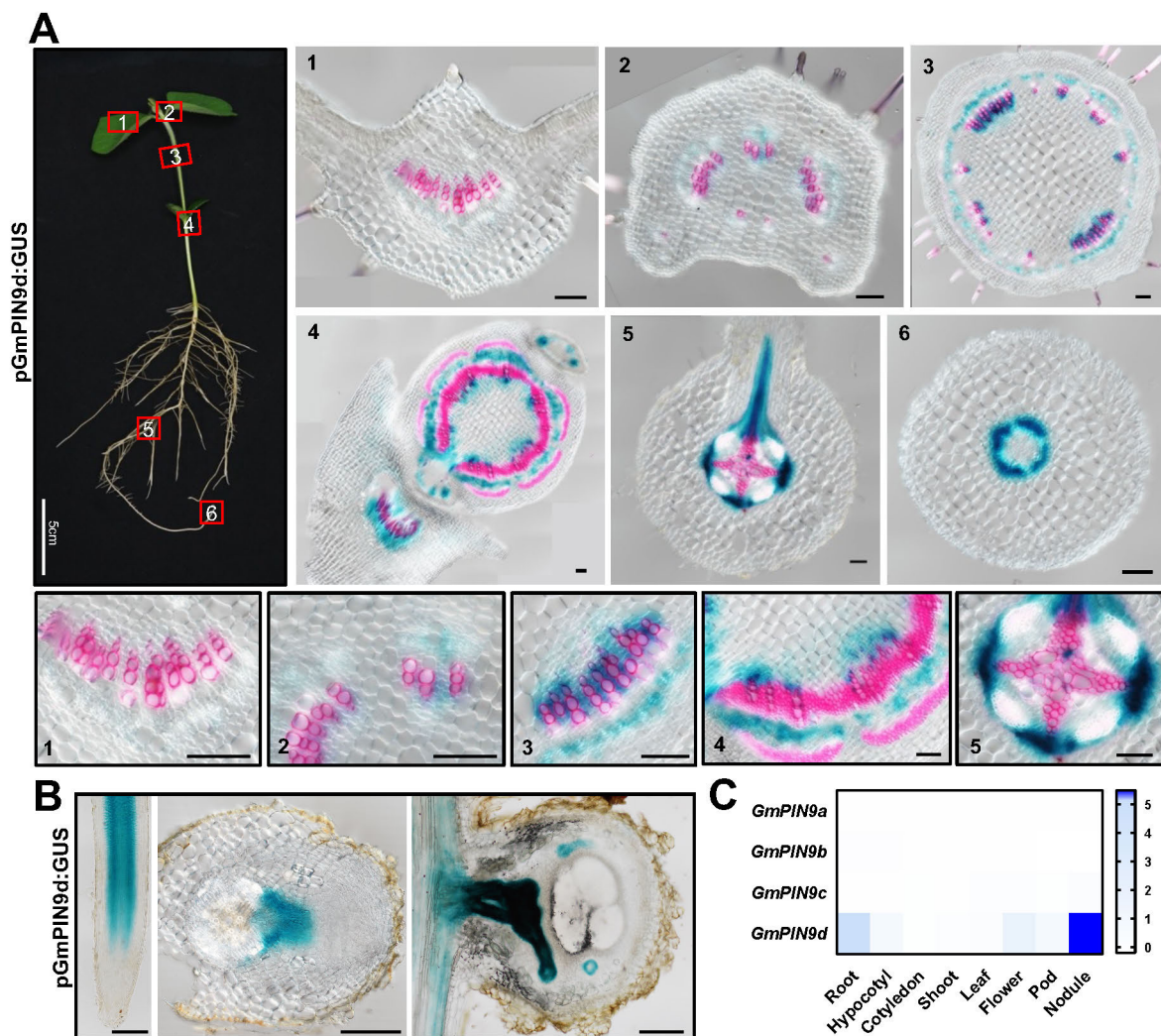


Figure 7. *GmPIN9d* is specifically expressed in the protoxylem cells of vascular bundles and root-nodule junctions.

(A) Different tissues of 10-day-old *pGmPIN9d:GUS* transgenic soybean plants were in series collected for sectioning and histochemical staining. Xylem cells were indicated by phloroglucin co-staining. Numbers in the right and lower panels indicated the areas labelled in the left image. Pictures in the lower panels showed 3× enlarged views of the images in the upper panels.

(B) *pGmPIN9d:GUS* transgenic soybean plants were infected by *BXYD3*, roots and different stages of nodules were collected for sectioning and histochemical staining.

(C) Transcript level of *GmPIN9a*, *b*, *c*, *d* genes was detected in different soybean tissues by RT-qPCR, and *Gmactin11* was used as the normalization gene. The relative transcript was shown by heatmap.

Scale bars, 100µm (A) and 200µm (B).

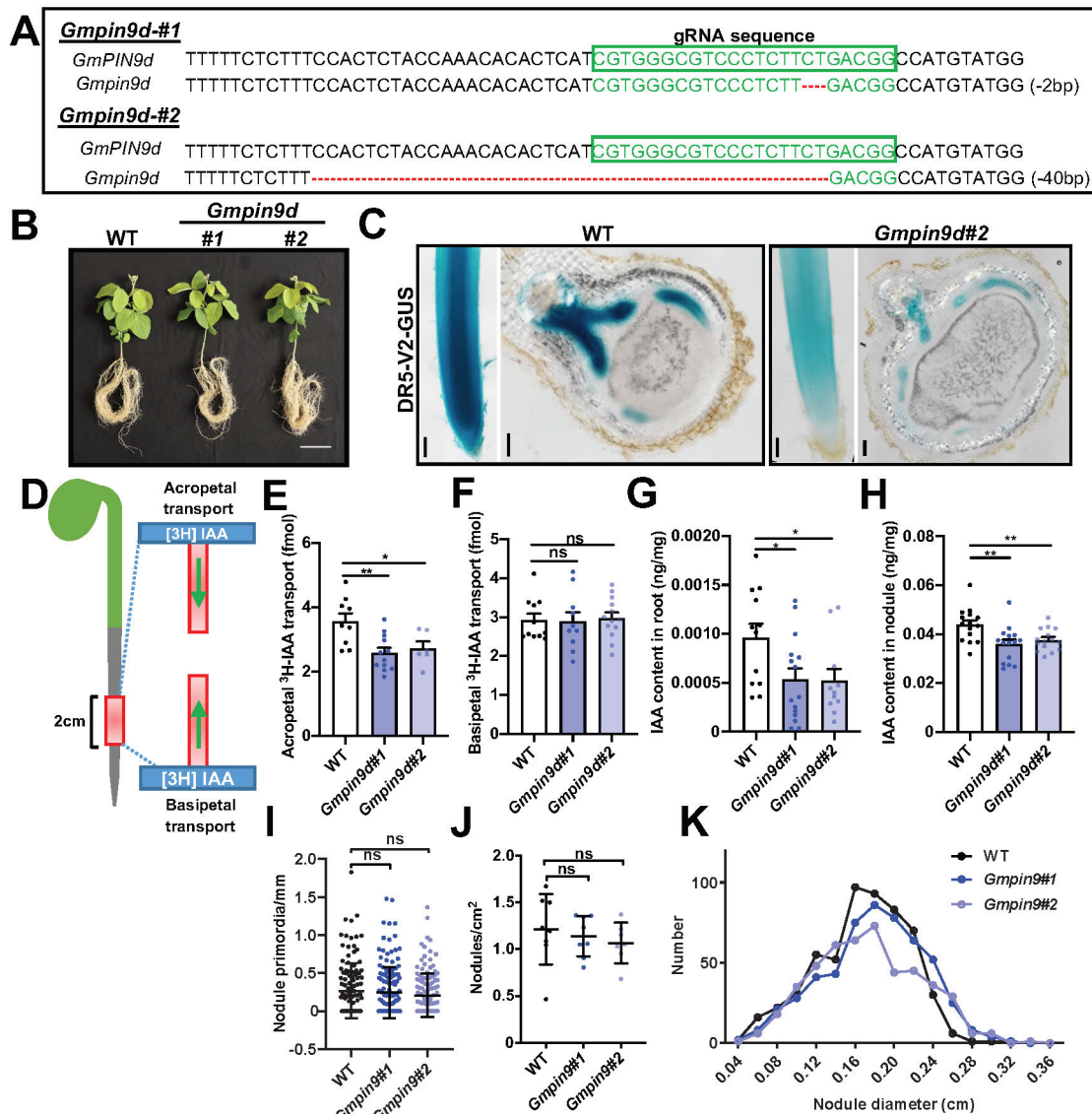


Figure 8. GmPIN9d transports auxin in an acropetal direction.

(A) *Gmpin9d* mutants were generated via CRISPR-Cas9 gene editing approach. gRNA targeted sites of *GmPIN9d* were framed by green, and the mutation or deletion sequences were labelled by red. Two independent mutant lines with editing manner were shown.

(B) Global morphology of 21-day-old *Gmpin9d* mutants.

(C) *DR5-V2-GUS* construct was introduced in WT, *Gmpin9d*#2 mutant background by hairy root transformation, and the positive hairy roots were infected by *BXYD3*. Roots and nodules were collected at 14dpi for sectioning and histochemical staining.

(D-F) Auxin transport capacity of WT and *Gmpin9d* mutants was assayed in 2cm root segments as described in D, and acropetal and basipetal auxin transportation were tracked by [³H]-IAA (n=9, 12, 6 in E; n=11, 10, 13 in F).

(G-H) Free IAA level was individually measured in the roots and nodules of WT and *Gmpin9d* mutants (G: n=12, 15, 11; H: n=15, 15, 15).

(I-K) 7-day-old WT and *Gmpin9d* mutants were infected by *BXYD3*. The nodule primordium density was analyzed at 6dpi (I: n=121, 137, 129), the nodule density was measured at 14dpi (J: n=8, 8, 7), and the profile of nodule diameter was tracked (K: n=560, 536, 473).

Scale bars, 10cm (B), 100 μ m (C). Error bar=S.E.M in E-H, S.D. in I, J. P-values were determined by two-tailed Student's t-test assuming equal variances (*p< 0.05; **p< 0.01; ns, not significant).

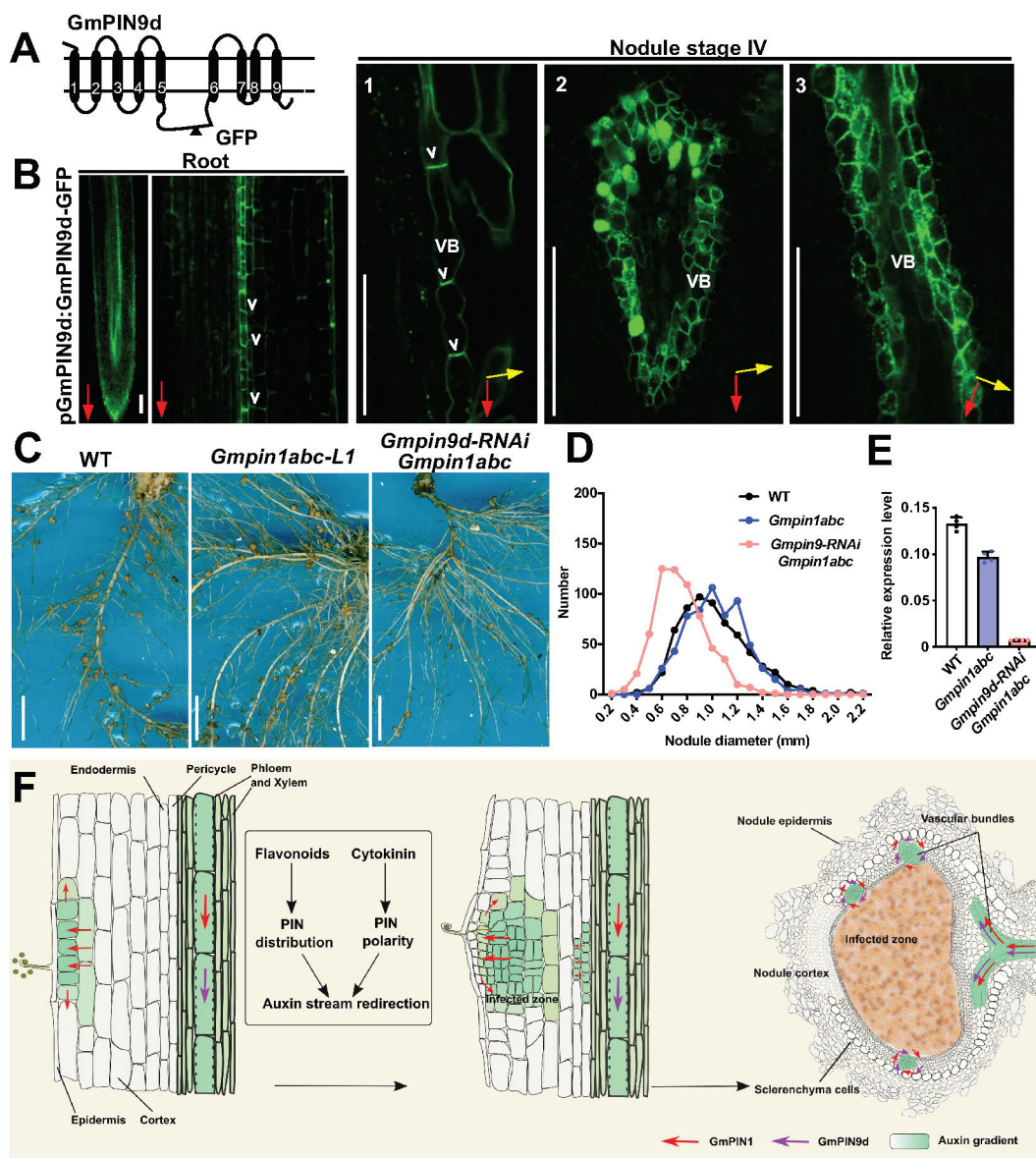


Figure 9. GmPIN9d works synergistically with GmPIN1 to coordinate nodule enlargement.

(A) GmPIN9d-GFP construct was established based on the insertion position of GFP in the hydrophilic loop. (B) *pGmPIN9d:GmPIN9d-GFP* construct was introduced in WT soybean plant by hairy root transformation, and the positive roots were infected by *BXYD3*. Roots and nodules were collected at 14dpi for sectioning, and GmPIN9d-GFP signal was visualized. Cells with polar GmPIN9d was highlighted by white arrows. The numbered images showed 5 \times enlarged views (red boxes framed) in Supp.Fig. 11G images. Root tip growth directions were labelled by red arrows, and directions of nodule apex were indicated by yellow arrows. VB, vascular bundle. (C-E) WT and *Gmpin1abc* mutants were transformed by *Gmpin9d-RNAi* construct (with dTomato-tag). The positive hairy roots were selected based on fluorescence and further infected by *BXYD3*, and the profile of nodule diameter was tracked in D (n=613, 618, 624) at 14dpi. Expression level of *GmPIN9d* was detected by RT-qPCR (E, n=4), *Gmactin11* was used as the normalization gene (E). (F) Model for polar auxin transport in nodule primordium and developing nodule. Stage I, GmPIN1 mainly directs auxin flow to the outer cortical cells, and partial auxin flows away from outer cortical cells. Stage II and III: GmPIN1-dependent auxin stream flows towards the nodule primordium, and partial auxin is retrieved to the neighboring cells. Stage IV: auxin stream is transported within vascular bundles towards nodule via GmPIN1 and GmPIN9d-dependent polar auxin transport. Auxin accumulations are depicted in green, auxin gradient is indicated by light green, and the presumptive routes of auxin flow are depicted by arrows (red arrows: GmPIN1-mediation; purple arrows: GmPIN9d-mediation). Flavonoid and cytokinin act as the elicitors to mediate rapid auxin stream redirection.

Scale bars, 100 μ m (B), 1cm (C). Error bar=S.D.

Parsed Citations

- Abas, L., Kolb, M., Stadlmann, J., Janacek, D.P., Lukic, K., Schwechheimer, C., Sazanov, L.A., Mach, L., Friml, J., and Hammes, U.Z. (2021). Naphthylphthalamic acid associates with and inhibits PIN auxin transporters. *Proc Natl Acad Sci U S A* 118.
Google Scholar: [Author Only](#) [Title Only](#) [Author and Title](#)
- Adamowski, M., and Friml, J. (2015). PIN-dependent auxin transport: action, regulation, and evolution. *Plant Cell* 27, 20-32.
Google Scholar: [Author Only](#) [Title Only](#) [Author and Title](#)
- Bai, M., Yuan, J., Kuang, H., Gong, P., Li, S., Zhang, Z., Liu, B., Sun, J., Yang, M., Yang, L., Wang, D., Song, S., and Guan, Y. (2020). Generation of a multiplex mutagenesis population via pooled CRISPR-Cas9 in soya bean. *Plant Biotechnol J* 18, 721-731.
Google Scholar: [Author Only](#) [Title Only](#) [Author and Title](#)
- Bailey, T.L., Boden, M., Buske, F.A., Frith, M., Grant, C.E., Clementi, L., Ren, J., Li, W.W., and Noble, W.S. (2009). MEME SUITE: tools for motif discovery and searching. *Nucleic Acids Res* 37, W202-208.
Google Scholar: [Author Only](#) [Title Only](#) [Author and Title](#)
- Benkova, E., and Bielach, A. (2010). Lateral root organogenesis - from cell to organ. *Curr Opin Plant Biol* 13, 677-683.
Google Scholar: [Author Only](#) [Title Only](#) [Author and Title](#)
- Benkova, E., Michniewicz, M., Sauer, M., Teichmann, T., Seifertova, D., Jurgens, G., and Friml, J. (2003). Local, efflux-dependent auxin gradients as a common module for plant organ formation. *Cell* 115, 591-602.
Google Scholar: [Author Only](#) [Title Only](#) [Author and Title](#)
- Bozsoki, Z., Gysel, K., Hansen, S.B., Lironi, D., Kronauer, C., Feng, F., de Jong, N., Vinther, M., Kamble, M., Thygesen, M.B., Engholm, E., Kofoed, C., Fort, S., Sullivan, J.T., Ronson, C.W., Jensen, K.J., Blaise, M., Oldroyd, G., Stougaard, J., Andersen, K.R., and Radutoiu, S. (2020). Ligand-recognizing motifs in plant LysM receptors are major determinants of specificity. *Science* 369, 663-670.
Google Scholar: [Author Only](#) [Title Only](#) [Author and Title](#)
- Brown, D.E., Rashotte, A.M., Murphy, A.S., Normanly, J., Tague, B.W., Peer, W.A., Taiz, L., and Muday, G.K. (2001). Flavonoids act as negative regulators of auxin transport in vivo in arabidopsis. *Plant Physiol* 126, 524-535.
Google Scholar: [Author Only](#) [Title Only](#) [Author and Title](#)
- Buer, C.S., Kordbacheh, F., Truong, T.T., Hocart, C.H., and Djordjevic, M.A. (2013). Alteration of flavonoid accumulation patterns in transparent testa mutants disturbs auxin transport, gravity responses, and imparts long-term effects on root and shoot architecture. *Planta* 238, 171-189.
Google Scholar: [Author Only](#) [Title Only](#) [Author and Title](#)
- Cai, Z., Wang, Y., Zhu, L., Tian, Y., Chen, L., Sun, Z., Ullah, I., and Li, X. (2017). GmTIR1/GmAFB3-based auxin perception regulated by miR393 modulates soybean nodulation. *New Phytol* 215, 672-686.
Google Scholar: [Author Only](#) [Title Only](#) [Author and Title](#)
- Calvert, H.E., Pence, M.K., Pierce, M., Malik, N.S.A., and Bauer, W.D. (1984). Anatomical analysis of the development and distribution of Rhizobium infections in soybean roots. *Canadian Journal of Botany* 62, 2375-2384.
Google Scholar: [Author Only](#) [Title Only](#) [Author and Title](#)
- Chen, X., Irani, N.G., and Friml, J. (2011). Clathrin-mediated endocytosis: the gateway into plant cells. *Curr Opin Plant Biol* 14, 674-682.
Google Scholar: [Author Only](#) [Title Only](#) [Author and Title](#)
- Du, M., Spalding, E.P., and Gray, W.M. (2020). Rapid Auxin-Mediated Cell Expansion. *Annu Rev Plant Biol* 71, 379-402.
Google Scholar: [Author Only](#) [Title Only](#) [Author and Title](#)
- Feraru, E., and Friml, J. (2008). PIN polar targeting. *Plant Physiol* 147, 1553-1559.
Google Scholar: [Author Only](#) [Title Only](#) [Author and Title](#)
- Friml, J., Wisniewska, J., Benkova, E., Mendgen, K., and Palme, K. (2002). Lateral relocation of auxin efflux regulator PIN3 mediates tropism in Arabidopsis. *Nature* 415, 806-809.
Google Scholar: [Author Only](#) [Title Only](#) [Author and Title](#)
- Galweiler, L., Guan, C., Muller, A., Wisman, E., Mendgen, K., Yephremov, A., and Palme, K. (1998). Regulation of polar auxin transport by AtPIN1 in Arabidopsis vascular tissue. *Science* 282, 2226-2230.
Google Scholar: [Author Only](#) [Title Only](#) [Author and Title](#)
- Gauthier-Coles, C., White, R.G., and Mathesius, U. (2018). Nodulating Legumes Are Distinguished by a Sensitivity to Cytokinin in the Root Cortex Leading to Pseudonodule Development. *Front Plant Sci* 9, 1901.
Google Scholar: [Author Only](#) [Title Only](#) [Author and Title](#)
- Geldner, N., Anders, N., Wolters, H., Keicher, J., Kornberger, W., Muller, P., Delbarre, A., Ueda, T., Nakano, A., and Jurgens, G. (2003). The Arabidopsis GNOM ARF-GEF mediates endosomal recycling, auxin transport, and auxin-dependent plant growth. *Cell* 112, 219-230.
Google Scholar: [Author Only](#) [Title Only](#) [Author and Title](#)
- Hirsch, A.M., Bhuvaneshwari, T.V., Torrey, J.G., and Bisseling, T. (1989). Early nodulin genes are induced in alfalfa root outgrowths elicited by auxin transport inhibitors. *Proc Natl Acad Sci U S A* 86, 1244-1248.

Google Scholar: [Author Only](#) [Title Only](#) [Author and Title](#)

Ip, H., D'Aoust, F., Begum, A.A., Zhang, H., Smith, D.L., Driscoll, B.T., and Charles, T.C. (2001). Bradyrhizobium japonicum mutants with enhanced sensitivity to genistein resulting in altered nod gene regulation. *Mol Plant Microbe Interact* 14, 1404-1410.

Google Scholar: [Author Only](#) [Title Only](#) [Author and Title](#)

Kereszt, A., Li, D., Indrasumunar, A., Nguyen, C.D., Nontachaiyapoom, S., Kinkema, M., and Gresshoff, P.M. (2007). Agrobacterium rhizogenes-mediated transformation of soybean to study root biology. *Nat Protoc* 2, 948-952.

Google Scholar: [Author Only](#) [Title Only](#) [Author and Title](#)

Kohlen, W., Ng, J.L.P., Deinum, E.E., and Mathesius, U. (2018). Auxin transport, metabolism, and signalling during nodule initiation: indeterminate and determinate nodules. *J Exp Bot* 69, 229-244.

Google Scholar: [Author Only](#) [Title Only](#) [Author and Title](#)

Kuhn, B.M., Nodzynski, T., Errafi, S., Bucher, R., Gupta, S., Aryal, B., Dobrev, P., Bigler, L., Geisler, M., Zazimalova, E., Friml, J., and Ringli, C. (2017). Flavonol-induced changes in PIN2 polarity and auxin transport in the Arabidopsis thaliana rol1-2 mutant require phosphatase activity. *Sci Rep* 7, 41906.

Google Scholar: [Author Only](#) [Title Only](#) [Author and Title](#)

Kumar, S., Stecher, G., Li, M., Knyaz, C., and Tamura, K. (2018). MEGAX: Molecular Evolutionary Genetics Analysis across Computing Platforms. *Mol Biol Evol* 35, 1547-1549.

Google Scholar: [Author Only](#) [Title Only](#) [Author and Title](#)

Kurepa, J., Shull, T.E., and Smalle, J.A. (2019). Antagonistic activity of auxin and cytokinin in shoot and root organs. *Plant Direct* 3, e00121.

Google Scholar: [Author Only](#) [Title Only](#) [Author and Title](#)

Laffont, C., Ivanovici, A., Gautrat, P., Brault, M., Djordjevic, M.A., and Frugier, F. (2020). The NIN transcription factor coordinates CEP and CLE signaling peptides that regulate nodulation antagonistically. *Nat Commun* 11, 3167.

Google Scholar: [Author Only](#) [Title Only](#) [Author and Title](#)

Lang, K., Lindemann, A., Hauser, F., and Gottfert, M. (2008). The genistein stimulon of Bradyrhizobium japonicum. *Mol Genet Genomics* 279, 203-211.

Google Scholar: [Author Only](#) [Title Only](#) [Author and Title](#)

Larkin, M.A., Blackshields, G., Brown, N.P., Chenna, R., McGettigan, P.A., McWilliam, H., Valentin, F., Wallace, I.M., Wilm, A., Lopez, R., Thompson, J.D., Gibson, T.J., and Higgins, D.G. (2007). Clustal W and Clustal X version 2.0. *Bioinformatics* 23, 2947-2948.

Google Scholar: [Author Only](#) [Title Only](#) [Author and Title](#)

Lewis, D.R., and Muday, G.K. (2009). Measurement of auxin transport in Arabidopsis thaliana. *Nat Protoc* 4, 437-451.

Google Scholar: [Author Only](#) [Title Only](#) [Author and Title](#)

Liao, C.Y., Smet, W., Brunoud, G., Yoshida, S., Vernoux, T., and Weijers, D. (2015). Reporters for sensitive and quantitative measurement of auxin response. *Nat Methods* 12, 207-210, 202 p following 210.

Google Scholar: [Author Only](#) [Title Only](#) [Author and Title](#)

Liu, C.W., and Murray, J.D. (2016). The Role of Flavonoids in Nodulation Host-Range Specificity: An Update. *Plants (Basel)* 5, 33.

Google Scholar: [Author Only](#) [Title Only](#) [Author and Title](#)

Livingston, D., Tuong, T., Nogueira, M., and Sinclair, T. (2019). Three-dimensional reconstruction of soybean nodules provides an update on vascular structure. *Am J Bot* 106, 507-513.

Google Scholar: [Author Only](#) [Title Only](#) [Author and Title](#)

Marhavy, P., Duclercq, J., Weller, B., Feraru, E., Bielach, A., Offringa, R., Friml, J., Schwechheimer, C., Murphy, A., and Benkova, E. (2014). Cytokinin controls polarity of PIN1-dependent auxin transport during lateral root organogenesis. *Curr Biol* 24, 1031-1037.

Google Scholar: [Author Only](#) [Title Only](#) [Author and Title](#)

Mashiguchi, K., Tanaka, K., Sakai, T., Sugawara, S., Kawaide, H., Natsume, M., Hanada, A., Yaeno, T., Shirasu, K., Yao, H., McSteen, P., Zhao, Y., Hayashi, K., Kamiya, Y., and Kasahara, H. (2011). The main auxin biosynthesis pathway in Arabidopsis. *Proc Natl Acad Sci U S A* 108, 18512-18517.

Google Scholar: [Author Only](#) [Title Only](#) [Author and Title](#)

Mathesius, U., Schlaman, H.R., Spaink, H.P., Of Sautter, C., Rolfe, B.G., and Djordjevic, M.A. (1998). Auxin transport inhibition precedes root nodule formation in white clover roots and is regulated by flavonoids and derivatives of chitin oligosaccharides. *The Plant journal : for cell and molecular biology* 14, 23-34.

Google Scholar: [Author Only](#) [Title Only](#) [Author and Title](#)

Mravec, J., Kubes, M., Bielach, A., Gaykova, V., Petrasek, J., Skupa, P., Chand, S., Benkova, E., Zazimalova, E., and Friml, J. (2008). Interaction of PIN and PGP transport mechanisms in auxin distribution-dependent development. *Development* 135, 3345-3354.

Google Scholar: [Author Only](#) [Title Only](#) [Author and Title](#)

Muller, A., Guan, C., Galweiler, L., Tanzler, P., Huijser, P., Marchant, A., Parry, G., Bennett, M., Wisman, E., and Palme, K. (1998). AtPIN2 defines a locus of Arabidopsis for root gravitropism control. *EMBO J* 17, 6903-6911.

Google Scholar: [Author Only](#) [Title Only](#) [Author and Title](#)

- Murray, J.D., Karas, B.J., Sato, S., Tabata, S., Amyot, L., and Szczyglowski, K. (2007). A cytokinin perception mutant colonized by *Rhizobium* in the absence of nodule organogenesis. *Science* 315, 101-104.
Google Scholar: [Author Only Title Only Author and Title](#)
- Ng, J.L., Hassan, S., Truong, T.T., Hocart, C.H., Laffont, C., Frugier, F., and Mathesius, U. (2015). Flavonoids and Auxin Transport Inhibitors Rescue Symbiotic Nodulation in the *Medicago truncatula* Cytokinin Perception Mutant *cre1*. *Plant Cell* 27, 2210-2226.
Google Scholar: [Author Only Title Only Author and Title](#)
- Ng, J.L.P., and Mathesius, U. (2018). Acropetal Auxin Transport Inhibition Is Involved in Indeterminate But Not Determinate Nodule Formation. *Front Plant Sci* 9, 169.
Google Scholar: [Author Only Title Only Author and Title](#)
- Okada, K., Ueda, J., Komaki, M.K., Bell, C.J., and Shimura, Y. (1991). Requirement of the Auxin Polar Transport System in Early Stages of *Arabidopsis* Floral Bud Formation. *Plant Cell* 3, 677-684.
Google Scholar: [Author Only Title Only Author and Title](#)
- Pacios-Bras, C., Schlaman, H.R., Boot, K., Admiraal, P., Langerak, J.M., Stougaard, J., and Spaink, H.P. (2003). Auxin distribution in *Lotus japonicus* during root nodule development. *Plant Mol Biol* 52, 1169-1180.
Google Scholar: [Author Only Title Only Author and Title](#)
- Peer, W.A., Bandyopadhyay, A., Blakeslee, J.J., Makam, S.N., Chen, R.J., Masson, P.H., and Murphy, A.S. (2004). Variation in expression and protein localization of the PIN family of auxin efflux facilitator proteins in flavonoid mutants with altered auxin transport in *Arabidopsis thaliana*. *Plant Cell* 16, 1898-1911.
Google Scholar: [Author Only Title Only Author and Title](#)
- Petrasek, J., Mravec, J., Bouchard, R., Blakeslee, J.J., Abas, M., Seifertova, D., Wisniewska, J., Tadele, Z., Kubes, M., Covanova, M., Dhonukshe, P., Skupa, P., Benkova, E., Perry, L., Krecek, P., Lee, O.R., Fink, G.R., Geisler, M., Murphy, A.S., Luschnig, C., Zazimalova, E., and Friml, J. (2006). PIN proteins perform a rate-limiting function in cellular auxin efflux. *Science* 312, 914-918.
Google Scholar: [Author Only Title Only Author and Title](#)
- Pierre-Jerome, E., Drapek, C., and Benfey, P.N. (2018). Regulation of Division and Differentiation of Plant Stem Cells. *Annu Rev Cell Dev Biol* 34, 289-310.
Google Scholar: [Author Only Title Only Author and Title](#)
- Popp, C., and Ott, T. (2011). Regulation of signal transduction and bacterial infection during root nodule symbiosis. *Curr Opin Plant Biol* 14, 458-467.
Google Scholar: [Author Only Title Only Author and Title](#)
- Qi, J., Wang, Y., Yu, T., Cunha, A., Wu, B., Vernoux, T., Meyerowitz, E., and Jiao, Y. (2014). Auxin depletion from leaf primordia contributes to organ patterning. *Proc Natl Acad Sci U S A* 111, 18769-18774.
Google Scholar: [Author Only Title Only Author and Title](#)
- Reid, D., Nadzieja, M., Novak, O., Heckmann, A.B., Sandal, N., and Stougaard, J. (2017). Cytokinin Biosynthesis Promotes Cortical Cell Responses during Nodule Development. *Plant Physiol* 175, 361-375.
Google Scholar: [Author Only Title Only Author and Title](#)
- Rightmyer, A.P., and Long, S.R. (2011). Pseudonodule formation by wild-type and symbiotic mutant *Medicago truncatula* in response to auxin transport inhibitors. *Mol Plant Microbe Interact* 24, 1372-1384.
Google Scholar: [Author Only Title Only Author and Title](#)
- Santelia, D., Henrichs, S., Vincenzetti, V., Sauer, M., Bigler, L., Klein, M., Bailly, A., Lee, Y., Friml, J., Geisler, M., and Martinoia, E. (2008). Flavonoids redirect PIN-mediated polar auxin fluxes during root gravitropic responses. *J Biol Chem* 283, 31218-31226.
Google Scholar: [Author Only Title Only Author and Title](#)
- Schaller, G.E., Bishopp, A., and Kieber, J.J. (2015). The yin-yang of hormones: cytokinin and auxin interactions in plant development. *Plant Cell* 27, 44-63.
Google Scholar: [Author Only Title Only Author and Title](#)
- Schiessl, K., Lilley, J.L.S., Lee, T., Tamvakis, I., Kohlen, W., Bailey, P.C., Thomas, A., Luptak, J., Ramakrishnan, K., Carpenter, M.D., Mysore, K.S., Wen, J., Ahnert, S., Grieneisen, V.A., and Oldroyd, G.E.D. (2019). NODULE INCEPTION Recruits the Lateral Root Developmental Program for Symbiotic Nodule Organogenesis in *Medicago truncatula*. *Curr Biol* 29, 3657-3668 e3655.
Google Scholar: [Author Only Title Only Author and Title](#)
- Stepanova, A.N., Yun, J., Robles, L.M., Novak, O., He, W., Guo, H., Ljung, K., and Alonso, J.M. (2011). The *Arabidopsis* YUCCA1 flavin monooxygenase functions in the indole-3-pyruvic acid branch of auxin biosynthesis. *Plant Cell* 23, 3961-3973.
Google Scholar: [Author Only Title Only Author and Title](#)
- Subramanian, S., Stacey, G., and Yu, O. (2006). Endogenous isoflavones are essential for the establishment of symbiosis between soybean and *Bradyrhizobium japonicum*. *The Plant journal : for cell and molecular biology* 48, 261-273.
Google Scholar: [Author Only Title Only Author and Title](#)
- Subramanian, S., Stacey, G., and Yu, O. (2007). Distinct, crucial roles of flavonoids during legume nodulation. *Trends Plant Sci* 12, 282-285.

Google Scholar: [Author Only](#) [Title Only](#) [Author and Title](#)

Suzaki, T., and Kawaguchi, M. (2014). Root nodulation: a developmental program involving cell fate conversion triggered by symbiotic bacterial infection. *Curr Opin Plant Biol* 21, 16-22.

Google Scholar: [Author Only](#) [Title Only](#) [Author and Title](#)

Suzaki, T., Yano, K., Ito, M., Umehara, Y., Suganuma, N., and Kawaguchi, M. (2012). Positive and negative regulation of cortical cell division during root nodule development in *Lotus japonicus* is accompanied by auxin response. *Development* 139, 3997-4006.

Google Scholar: [Author Only](#) [Title Only](#) [Author and Title](#)

Teale, W.D., Pasternak, T., Dal Bosco, C., Dovzhenko, A., Kratzat, K., Bildl, W., Schworer, M., Falk, T., Ruperti, B., Schaefer, J.V., Shahriari, M., Pilgermayer, L., Li, X., Lubben, F., Pluckthun, A., Schulte, U., and Palme, K. (2021). Flavonol-mediated stabilization of PIN efflux complexes regulates polar auxin transport. *EMBO J* 40, e104416.

Google Scholar: [Author Only](#) [Title Only](#) [Author and Title](#)

Turner, M., Nizampatnam, N.R., Baron, M., Coppin, S., Damodaran, S., Adhikari, S., Arunachalam, S.P., Yu, O., and Subramanian, S. (2013). Ectopic expression of miR160 results in auxin hypersensitivity, cytokinin hyposensitivity, and inhibition of symbiotic nodule development in soybean. *Plant Physiol* 162, 2042-2055.

Google Scholar: [Author Only](#) [Title Only](#) [Author and Title](#)

Ulmasov, T., Murfett, J., Hagen, G., and Guilfoyle, T.J. (1997). Aux/IAA proteins repress expression of reporter genes containing natural and highly active synthetic auxin response elements. *Plant Cell* 9, 1963-1971.

Google Scholar: [Author Only](#) [Title Only](#) [Author and Title](#)

van Noorden, G.E., Kerim, T., Goffard, N., Wiblin, R., Pellerone, F.I., Rolfe, B.G., and Mathesius, U. (2007). Overlap of proteome changes in *Medicago truncatula* in response to auxin and *Sinorhizobium meliloti*. *Plant Physiol* 144, 1115-1131.

Google Scholar: [Author Only](#) [Title Only](#) [Author and Title](#)

Viaene, T., Delwiche, C.F., Rensing, S.A., and Friml, J. (2013). Origin and evolution of PIN auxin transporters in the green lineage. *Trends Plant Sci* 18, 5-10.

Google Scholar: [Author Only](#) [Title Only](#) [Author and Title](#)

Wang, Y., Chai, C., Valliyodan, B., Maupin, C., Annen, B., and Nguyen, H.T. (2015a). Genome-wide analysis and expression profiling of the PIN auxin transporter gene family in soybean (*Glycine max*). *BMC Genomics* 16, 951.

Google Scholar: [Author Only](#) [Title Only](#) [Author and Title](#)

Wang, Y., Yang, W., Zuo, Y., Zhu, L., Hastwell, A.H., Chen, L., Tian, Y., Su, C., Ferguson, B.J., and Li, X. (2019). GmYUC2a mediates auxin biosynthesis during root development and nodulation in soybean. *J Exp Bot* 70, 3165-3176.

Google Scholar: [Author Only](#) [Title Only](#) [Author and Title](#)

Wang, Y., Li, K., Chen, L., Zou, Y., Liu, H., Tian, Y., Li, D., Wang, R., Zhao, F., Ferguson, B.J., Gresshoff, P.M., and Li, X. (2015b). MicroRNA167-Directed Regulation of the Auxin Response Factors GmARF8a and GmARF8b Is Required for Soybean Nodulation and Lateral Root Development. *Plant Physiol* 168, 984-999.

Google Scholar: [Author Only](#) [Title Only](#) [Author and Title](#)

Weijers, D., Sauer, M., Meurette, O., Friml, J., Ljung, K., Sandberg, G., Hooykaas, P., and Offringa, R. (2005). Maintenance of embryonic auxin distribution for apical-basal patterning by PIN-FORMED-dependent auxin transport in *Arabidopsis*. *Plant Cell* 17, 2517-2526.

Google Scholar: [Author Only](#) [Title Only](#) [Author and Title](#)

Wisniewska, J., Xu, J., Seifertova, D., Brewer, P.B., Ruzicka, K., Blilou, I., Rouquie, D., Benkova, E., Scheres, B., and Friml, J. (2006). Polar PIN localization directs auxin flow in plants. *Science* 312, 883.

Google Scholar: [Author Only](#) [Title Only](#) [Author and Title](#)

Wu, C., Dickstein, R., Cary, A.J., and Norris, J.H. (1996). The Auxin Transport Inhibitor N-(1-Naphthyl)phthalamic Acid Elicits Pseudonodules on Nonnodulating Mutants of White Sweetclover. *Plant Physiol* 110, 501-510.

Google Scholar: [Author Only](#) [Title Only](#) [Author and Title](#)

Wu, M.F., Yamaguchi, N., Xiao, J., Bargmann, B., Estelle, M., Sang, Y., and Wagner, D. (2015). Auxin-regulated chromatin switch directs acquisition of flower primordium founder fate. *Elife* 4, e09269.

Google Scholar: [Author Only](#) [Title Only](#) [Author and Title](#)

Xiao, T.T., Schilderink, S., Moling, S., Deinum, E.E., Kondorosi, E., Franssen, H., Kulikova, O., Niebel, A., and Bisseling, T. (2014). Fate map of *Medicago truncatula* root nodules. *Development* 141, 3517-3528.

Google Scholar: [Author Only](#) [Title Only](#) [Author and Title](#)

Xiong, Y., and Jiao, Y. (2019). The Diverse Roles of Auxin in Regulating Leaf Development. *Plants (Basel)* 8, 243.

Google Scholar: [Author Only](#) [Title Only](#) [Author and Title](#)

Xu, J., and Scheres, B. (2005). Dissection of *Arabidopsis* ADP-RIBOSYLATION FACTOR 1 function in epidermal cell polarity. *Plant Cell* 17, 525-536.

Google Scholar: [Author Only](#) [Title Only](#) [Author and Title](#)

Yamaguchi, N., Wu, M.F., Winter, C.M., Berns, M.C., Nole-Wilson, S., Yamaguchi, A., Coupland, G., Krizek, B.A., and Wagner, D. (2013). A

molecular framework for auxin-mediated initiation of flower primordia. Dev Cell 24, 271-282.

Google Scholar: [Author Only](#) [Title Only](#) [Author and Title](#)

Yang, H., Wang, Y., Li, L., Li, F., He, Y., Wu, J., and Wei, C. (2019). Transcriptomic and Phytochemical Analyses Reveal Root-Mediated Resource-Based Defense Response to Leaf Herbivory by Ectropis oblique in Tea Plant (Camellia sinensis). J Agric Food Chem 67, 5465-5476.

Google Scholar: [Author Only](#) [Title Only](#) [Author and Title](#)

Zhang, J., Subramanian, S., Stacey, G., and Yu, O. (2009). Flavones and flavonols play distinct critical roles during nodulation of Medicago truncatula by Sinorhizobium meliloti. The Plant journal : for cell and molecular biology 57, 171-183.

Google Scholar: [Author Only](#) [Title Only](#) [Author and Title](#)

Zhang, J., Nodzynski, T., Pencik, A., Rolcik, J., and Friml, J. (2010). PIN phosphorylation is sufficient to mediate PIN polarity and direct auxin transport. Proc Natl Acad Sci U S A 107, 918-922.

Google Scholar: [Author Only](#) [Title Only](#) [Author and Title](#)

Zhang, X., Huang, X., Li, Y., Tao, F., Zhao, Q., and Li, W. (2021). Polar auxin transport May Be responsive to specific features of flavonoid structure. Phytochemistry 185, 112702.

Google Scholar: [Author Only](#) [Title Only](#) [Author and Title](#)

Zhao, Y. (2018). Essential Roles of Local Auxin Biosynthesis in Plant Development and in Adaptation to Environmental Changes. Annu Rev Plant Biol 69, 417-435.

Google Scholar: [Author Only](#) [Title Only](#) [Author and Title](#)